Problems of Planetology, Cosmochemistry and Meteoritica

Barenbaum A.A.On the scientific revolution in the cjmparative planetogy

Oil and Gas Research Institute RAS, Moscow

Abstract. Author considers that today in the Comparative Planetology is realized the transition to a new representations which are based on the Galactocentric paradigm. This paradigm considers the Sun and planets formation as a cyclical process in which comets and stars of Galaxy take part. We can distinguish two key events in Solar system formation. The main (6.6 billion years ago) has been connected with the birth of Sun and planets. And the second event (4.6 billion years ago) caused by the destruction of planet Phaeton, that led to a change in mass of the majority planets, as well as to emergence of satellites of planets, comets and asteroids. Both events took place in the same galactic branch "Perseus + 1" at a distance of radius corotation from the Galaxy center. We presented some conclusions the Galactocentric paradigm relating to processes on the second stage of Solar system formation.

Keywords: Comparative Planetology, Galactocentric paradigm, Solar system, Kant-Laplace cosmogony.

Citation: Barenbaum A.A. (2016). On the scientific revolution in the comparative planetology, Experimental geochemistry. (in press)

By definition [Florensky et al., 1981] Comparative planetology is the science that studies the Sun and planets as one natural system of cosmic bodies in aggregate of all their properties. Being closely related with cosmogony, geology, geochemistry and geophysics, Comparative planetology occupies its independent place in the cosmic natural science.

Analysis of the modern state of this science leads the author to the conclusion that today in Comparative planetology is happening scientific revolution [Kuhn, 1962]. The cause of the revolution has become a recent discovery in astronomy the fact of expiration of flows gas-dust matter from the nucleus our Galaxy [Barenbaum, 2002]. This astrophysical phenomenon lets to reveal the failure of the Kant-Laplace cosmogonical doctrine in the questions of the origin Solar system and its planets.

It is now firmly established [Barenbaum, 2010] that at the motion of Sun in Galaxy the all planets of Solar system through the 20-37 mln years are subject to intense bombardments by galactic comets and 1 billion times a year the Sun crosses the dense clusters of stars, dust and gas in the arms of Galaxy, which greatly affects the processes in Solar system and on its planets.

On the basis of these facts, the author proposed a new cosmogonical concept of formation and evolution of Solar system, which is called "The cosmogony of open Solar system (COSS)" [Barenbaum 1992, 2002, 2010]. Concept COSS is in contrast to the hypothesis of Kant-Laplace considers processes in Galaxy as a major factor defining the conditions formation and evolution of Sun and its planets.

Below are some provisions of the Concept COSS, that reflect the essence of the scientific revolution taking place in the Comparative planetology today.

- Origin of the Sun and the planets, this is not a one-time event, but a cyclical process, which since moment of the Solar system birth is abruptly intensified in the epochs when Sun is in the Galaxy branches.
- We can distinguish two main periods of formation of the Solar system. This is the era of emergence of the Sun and planets of 6.6 billion years ago. And the event of 4.6 billion years ago, with which we associate the second period of planets formation. Both events occurred [Barenbaum, 2015] in the spiral arm "Perceus + 1" [Vallee, 2002], in star-forming region in the distance of corotation radius from center of Galaxy [Barenbaum, 2010].
- The first event is well explained by the standard model of the Solar system formation [Vityazev et al., 1991]. While the second event which according to the Schmidt's hypothesis [Schmidt, 1957] led to formation the gas sheaths and the systems of satellites of giant planets is explained by the model [Barenbaum, 2010]. This model based on Olbers's hypothesis (1802) death of the planet Phaeton lets also explain origin of the asteroids belt and the observed comets [Barenbaum, 1990].
- According this model, the formation of belt asteroid bodies from Phaeton's fragments, which have become objects of intense collisions with galactic comets, has initiated four processes taking place in different areas of Solar system at the same time [Barenbaum, 1992]:

1) increase of Sun's mass by about half due to the capture a new cosmic matter;

2) evaporation and crushing of galactic comets at colliding with bodies of belt as well as mixing of substance of those and others;

3) ejection from asteroid belt large fragments of Phaeton which bombarded the planets;

4) emission out the zone belt of huge mass of gas and dust, resulting in epochs of cometary bombardments on the outside of asteroid belt formed "secondary" gas-dust disk of Sun, part substance of which was seized by planet-giants.

This model has allowed offering coordinated solutions for a row of cosmogony problems. Here are some of our findings:

- Prior to Phaeton destruction the masses of all planets are followed power dependence [Vityazev et al., 1990]. However after Phaeton destruction, many of planets have changed, that led to their separation into "internal" and "external". The outer planets: Jupiter, Saturn and Uranus, which turned inside the secondary disk of Sun, captured a new substance, which has become by their gas sheath, and have provided themselves by system of satellites. While the inner planets: Mars and Earth are lost their own mass.
- On destruction moment the Phaethon represented of self a planet terrestrial type with mass in 2.5 Earthly masses. As and modern the Earth, the Phaeton already had possessed by the five silicate shells as well as the inner Fe-Ni nucleus. The main difference in structures of both planets is that now our Earth has a more massive metallic nucleus and contains in mantle silicates less Fe than the Phaeton, which interrupted its evolution at an earlier stage.
- Phaeton's death also has led to appearance of satellite Earth – the Moon. Calculations show [Barenbaum, 1992a] that as a result of the falling large fragments of Phaeton, our planet is probably lost 245 ± 10 km of surface layer rocks consisting on 1/3 of primary crust and on 2/3 of mantle rocks. About 20% of this material has formed a ring on the near-Earth orbit and later entered into composition of Moon, and the rest was lost forever.
- This calculation confirms the hypothesis [Ringwood, 1988] that the origin of the Moon could be the result of fallout on the earth many smaller bodies, but not the Earth's collision with another large planet. That better fits the geochemistry data for the Earth and the Moon.
- Finally, another important conclusion concerning the origin comets of the Solar system:
- The comets that we see now are the products of collisions of galactic comets and asteroids captured on near-solar orbits. The vast majorities of such comets were born and were thrown out of the asteroid belt of 1÷5 million years ago during the last bombardment Solar system by galactic comets.
- The long-period comets having very large periods currently are finishing only the first its turnover around the Sun. Points aphelion orbit of such comets are located from the Sun at distance of (2–50)×10^3 AU, which determines the position of "cometary cloud" in the hypothesis of Oort.
- Thereby the Oort cloud is the concentration area of points aphelion orbits of comets Solar system, which were born in asteroid belt of 1-5 mln years ago and today returning to Sun. This "cometary Oort cloud" is the fiction. Of course, nothing to do with the formation of the solar system, it does not have [Barenbaum, 1990].

This article gives a sufficiently clear representation of the scientific revolution, which according to the author, is happening today in the comparative planetology.

References:

1. Barenbaum A.A. (1990). New ideas about the origin of comets and their interactions with the objects of Solar system. *Kometnyy tsirkulyar*. № 418, Kiev, pp. 11-12.
2. Barenbaum A.A. (1992) The origin of asteroids and meteorites (a new concept of cosmogony). *Conceptual bases of geology*. (St. Petersburg: SPb Mining institute), pp. 9-27.
3. Barenbaum A.A. (1992a) The Solar system in the Phaeton explosion era: Origin of the Moon. *Conceptual bases of geology*. (St. Petersburg: SPb Mining institute), pp. 95-106.
4. Barenbaum A.A. (2002) *The Galaxy, Solar System, Earth: Coordinated Processes and Evolution*. (Moscow: GEOS).
5. Barenbaum A.A. (2003) Confirmation of the hypothesis O.Yu. Schmidt about the nature of solid core of giant planets. *Vestnik Otdeleniya nauk o Zemle RAN*, №1(21) '2003. URL: http://www.scgis.ru/russian/cp1251/h_dggggms/1-2003//informbul-1_2003/ planet-6.pdf.
6. Barenbaum A.A. (2007) To the problem of internal structure and deep-seated evolution Earth. *Inform. Bulletin (ESEMPG-2007). Vestnik Otdeleniya nauk o Zemle RAN*-№1(25)′ 2007. http://www.scgis/rurussian/cp1251/hdgggms/1-2007/informbul-1/ hydroterm-24.pdf.
7. Barenbaum A.A. (2010) Galactocentric Paradigm in Geology and Astronomy (Moscow: LIBROKOM).
8. Barenbaum A.A. (2015) The Sun position in Galaxy in era of Phaeton destruction, *Proceedings of XVI Intl. Conf.: Physic-chemical and petrophysical studies in Earth Sciences*. (Moscow: IGEM RAS), pp. 39-42.
9. Florensky K.P., Bazilevsky A.T., Burba G.A. et al. (1981) *Essays on Comparative planetology*. (Moscow: Nauka).
10. Kuhn T.S. (1962) *The Structure of Scientific Revolutions*. (Chicago: Univer. of Chicago Press).
11. Ringwood A.E. (1988) Lunar origin: single giant impact or multiple large impacts? *Abstr. Paper 19-th*

Lunar and Planet. Sci. Conf., Houston. Pt. 3, pp. 982-983.
12. Schmidt O.Yu. (1957) *Four Lectures on Theory of Earth Origin*. (Moscow: USSR AS).
13. Vallee J.P. (2002) Metastudy of the spiral structure of our home Galaxy. *Astrophys. J.* V. 566. №1, pp. 261-266.
14. Vityazev A.B., Pechernikova G.V., Safronov V.S. (1990) *Terrestrial Planets: Origin and Early Evolution*. (Moscow: Nauka).

Basilevsky A.T.[1,2,3], Krasilnikov S.S.[1,2,3], Skripnik A.Ya.[1], Lorenz C.A.[1], Shiryaev A.A.[4,5], Mall U.[2], Keller H.U.[6], Skorov Yu.V.[2], Mottola S.[7], Hvid S.F.[7],[1] **Strength and texture of material of 67P comet nucleus based on the data taken by Rosetta mission.**

[1] GEOKHI RAN, Moscow, Russia;
[2] Max-Planck-Institute for Solar System Research, Göttingen, Germany;
[3] MIIGAIK, Moscow, Russia;
[4] Institute of Physical Chemistry & Electrochemistry, RAN, Moscow, Russia;
[5] IGEM RAN, Moscow, Russia;
[6] Institute for Geophysics & Extraterrestrial Physics, TU Braunschweig, Braunschweig, Germany;
[7] DLR Institute of Planetary Research, Berlin, Germany.

Abstract. From analysis of the 67P comet nucleus images taken by NavCam and ROLIS cameras and produced from the Preusker et al. (2015) shape model it was found that consolidated nucleus material outcropped at the Hathor cliff and in some other places, shows very low mechanical strength (comparable with that of fresh fallen snow at -10°C) and hierarchical graininess from the dekameter to sub-millimeter scales. The graininess seems to be due to material inhomogeneities in ability to resist to surface sublima-tional weathering that implies difference in content of volatiles. Very low mechanical strength suggests very weak grain-to-grain connections with no or very minor sintering by ice(s). All this suggests that the low strength and hierarchical graininess are inherited since formation of the comet body so since that time "classical" volatiles (H_2O, CO_2, CO,..) behaved essentially as "classical" solids.
UDC 523.64-823

Keywords: cometary nucleus, material strength, texture, 67P Churyumov-Gerasimenko.

Nucleus of comet 67P Churyumov-Gerasimenko (diameter ~4 km) consists of two parts, one of which is informally called Body, another one – Head, and connecting them Neck, whose one of slopes, the Hathor cliff, is almost vertical, with overhangs (Thomas et al., 2015) (Fig. 1).

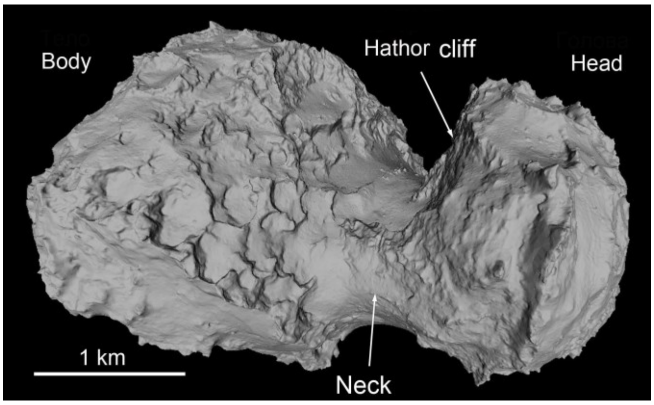

Fig.1. General view on comet 67P nucleus according to Shape model of Preusker et al. (2015).

Strength of the consolidated nucleus material was estimated from characteristics of relief of Hathor cliff and some other areas (Preusker et al., 2015), where it is outcropped (Groussin et al., 2015; Basilevsky et al., 2016): Tensile strength was found to be from 1.5 to 100 Pa, shear strength, from ~13 to ≥30 Pa, compressive strength, from 30 to 150 Pa, probably, to 1.5 kPa. Taking into account the dependence of measurements' results from the object size (Xu, 2005), they are close to those for dry fresh-fallen snow at -10°C (Fig. 2).

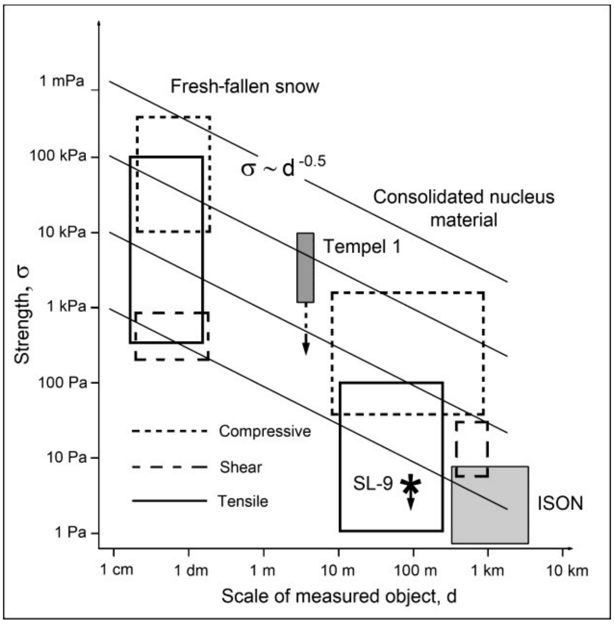

Fig.2. Strength of consolidated nucleus material of comet 67P in comparison with those of fresh-fallen snow. SL-9 is estimate of Asphaug & Benz (1999) of tensile strength of Shoemaker-Levy comet nucleus, grey rectangles – strengths of nuclei of comets ISON (Steckloff et al., 2015) and Tempel 1 (Richardson & Melosh, 2013). Inclined lines show dependence of results of the tensile and compressive strength measurements from the object size (Xu, 2005).

At the Hathor cliff and in some other areas where consolidated nucleus material is ourcropped, its "grainy" texture at the scale of a few decameters is seen (Fig. 3).

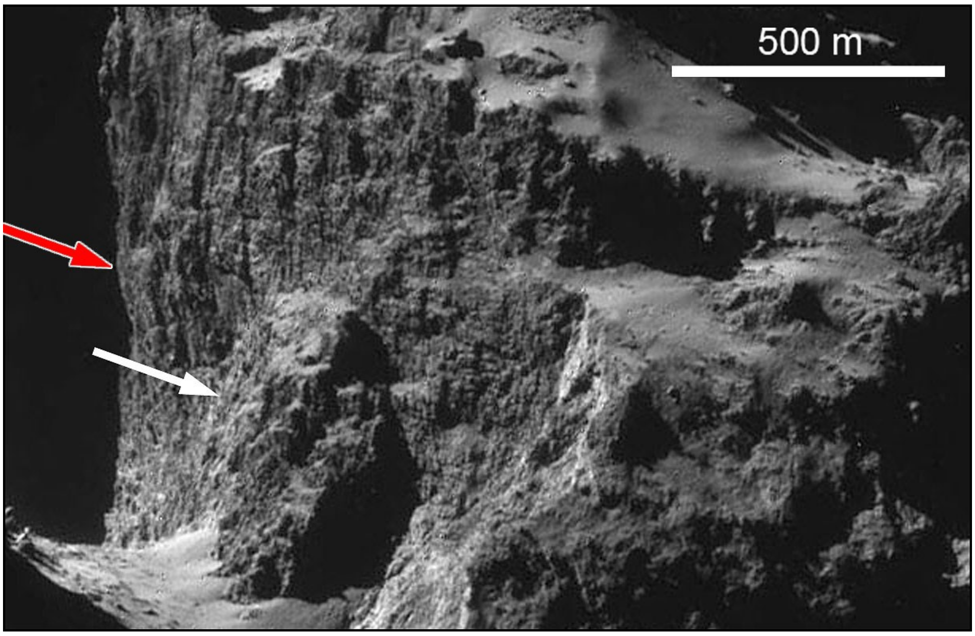

Fig.3. NavCam image of Hathor cliff with knobby (grainy) surface texture. In the lowe part of the slope a a body of landslide is seen (white arrow), in the moddle part is seen overhang (red arrow).

Grainy texture is seen also in fragments of consolidated nucleus material (Figure 4), but not in fresh breaks (upper images), but in those which suffered sublimational weathering (lower images).

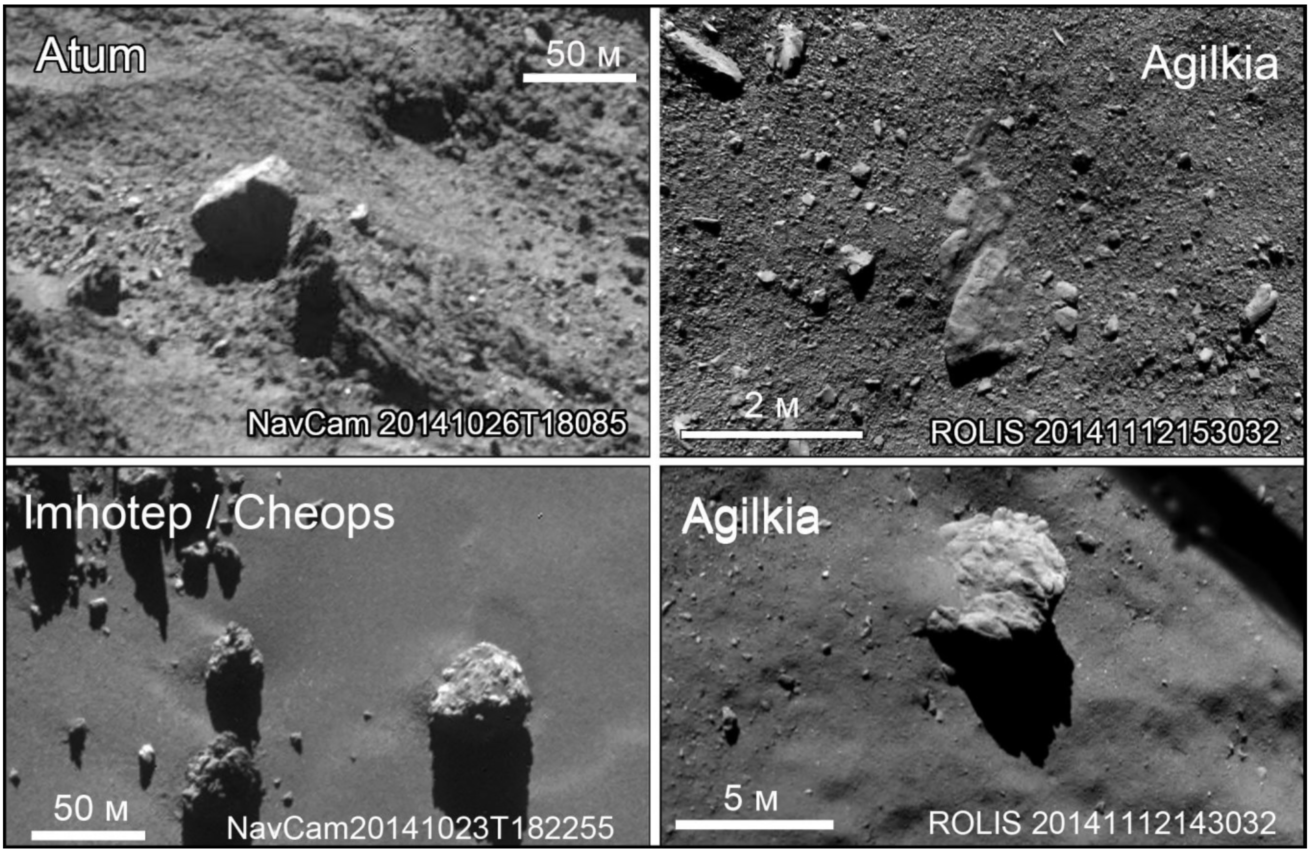

Fig. 4. Angular (above) and "rounded" (below) fragments of nucleus material.

Fine-grained texture of submillimeter scale is seen for the particles caught, in coma of this comet (e.g., Schulz et al., 2015; Langevin Y., et al. 2016).

The observed grainy texture could be inherent for the compact material being due to inhomogeneities of composing it parts in different resistance to sublimational weathering (e.g., difference in contents of volatiles). Or if the nucleus material is not compact, but is like "rubble-pile" (Weissman, 1986), that, however, does not agree with observations, for example., in Bastet region (Fig.5).

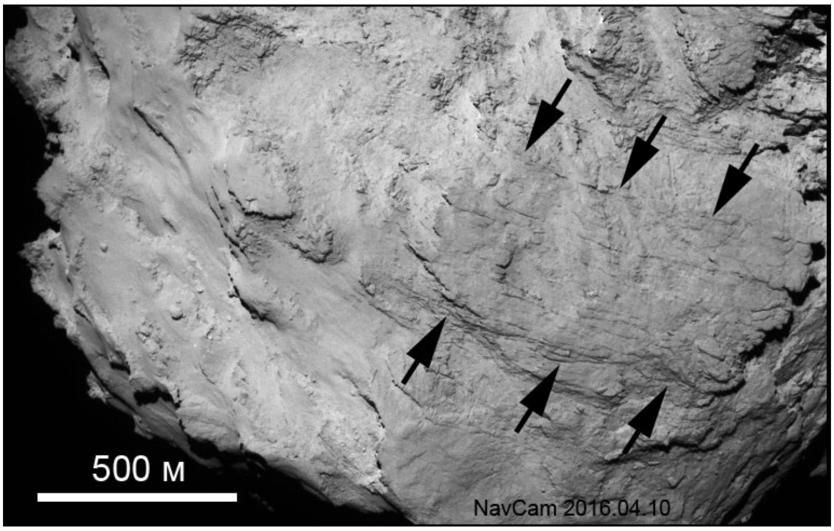

Fig.5. Presence of long lineaments contradicts to the "rubble-pile" veresion of nucleus.

Interesting, that stony material of asteroids of S type is mechanically more strong than the cometary one, and at the scales larger than centimeters is not grainy (Figure 6), that is probably due to fundamental differences in origin and subsequent evolution.

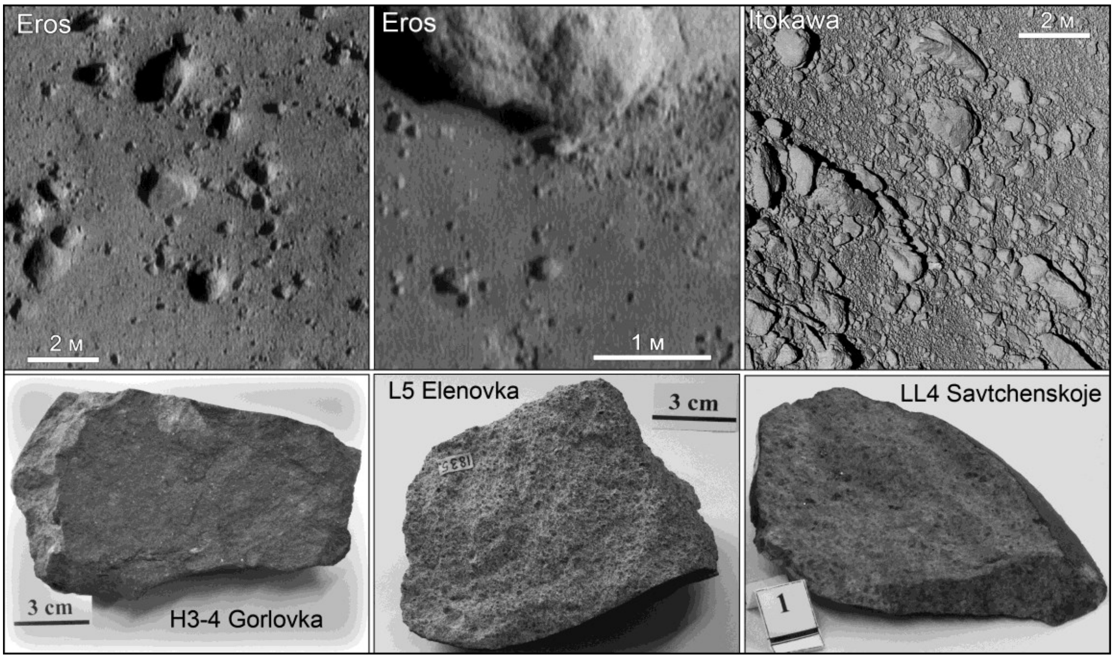

Fig.6. Above – fragments on the surface of S-asteroids Eros and Itokawa. Below – fragments of ordinary chondrites of H, L и LL types.

So, the consolidated nucleus material of 67P comet has very low mechanical strength and hierarchical "graininess" from decameters to submillimeter sizes. The graininess is probably due to inhomogeneity of this material in some characteristics, including, in contents of volatiles. Very low mechanical strength suggests weak grain-to-grain bonds without freezing at contacts. These characteristics seem to be inherited since the time of nucleus formation, that implies, that since that time the "classical" volatiles (H_2O, CO_2, CO...) behaved as "classical" solids.

This work was partly supported by the Humbold Foundation (A.T. Basilevsky – geological analysis of images of 67P comet), by Russian Science Foundatio, Project No 14-22-00197 (A.T. Basilevsky, S.S. Krasilnikov – morphometric analysis of the nucleus surface), by Program 7 (9) of Russian Academy Presidium (A.T. Basilevsky, S.S. Krasilnikov – comparisons with landforms of other bodies) and by the RFBR Grant 15-05-03351 (A.A. Shiryaev - comparisons of fractures formed in various loose materials).

References:

1. Asphaug E., Benz W., 1996. Icarus, 121.
2. Basilevsky A. et al. 2016. LPSC-47, abs # 1215.
3. Groussin O. et al. 2015. Astr. & Astrophys. 583.
4. Langevin Y., et al. 2016. Icarus. 271.
5. Preusker F., et al. 2015. Astr. & Astrophys. 583.
6. Richardson J., Melosh H. 2013. Icarus. 222.
7. Schulz R. et al. 2015. Nature. 518.
8. Steckloff J. et al., 2015. Icarus. 258.
9. Thomas N. 2015. Science. 347 (6220).
10. Weissman, P.R., 1986. Nature. 320.
11. Xu P. 2005. Mechanics Research Communications. 32

Yurkovets V.P. Moissanite in rocks of the Ladoga area as an indicator of the Ladoga impact.

The Academy of DNA Genealogy, Boston, USA
(valery.yurkovets@gmail.com)

Abstract. The paper provides with a model of three-phase formation of moissanite in impactites of Ladoga impact volcanic structure. Polycrystalline silicon carbide is formed in melting zone of shungite-bearing quartzitic shales at the first stage. Its sublimation by expanding vapour phase of impact (vapour rocks) heated to tens of thousands of degrees, occurs at the second stage. Subsequent crystallization of moissanite from the vapor which continues to expand, happens at the third stage as a result of adiabatic cooling of fireball.

Keywords: moissanite, Ladoga impact volcanic structure, shock microstructures, shungite.

One of the distinctive features of the Ladoga impact, along with the shock microstructures (ShM) which are unique yet, is anomalous wide spreading of moissanite in the impactites of the Ladoga impact-volcanic structure. Moissanite of 6H and 15R polytypes was found in the fragments of allogeneic breccia rocks sampled inside impact crater and in the catastrophic layers uncovered outside it. The distance between the outermost points of moissanite findings is about 160 kilometers, from Priozersk in the north-west of the Lake Ladoga to Kirsino-Shapkino kames in the south of Ladoga area. In all samples moissanite is present in the upper layer in the center of ShM, represented by concentric zones of melting and (or) crushing mineral grains of target. Inside the crater shock microstructures were found in the Vendian sandstone fragments of which in particular allogeneic breccia consists. In the catastrophic layers they were found in Cambrian and Vendian sandstone boulders and pebbles. [Yurkovets V. P., 2014a].

All ShM and moissanite findings outside the impact crater are in ferruginous inclusions formed as a result of an inelastic impact of melt particles with a high kinetic energy. Fig. 1 shows as an example samples N 164 and 259 of sandstone pebble with small ferruginous inclusions. In Fig. 2 photos of some parts of thin section of sample N 259 are shown. Quartz out of inclusions composes about 80%, it has no signs of impact, is well-rounded, cement is contact (photo 1). In place of impact melt hitting cement is ferruginous, grains are fragmented, quartz has a cloudy extinction (photo 2), indicating a strong stress resulted in deformation of crystal structure. At the boundary of melting and enclosing mass of sandstone it is typical presence of Impact spallation occurring when grain stressing by impulse reflection [Ernstson and Claudin, 2011], which confirms the impact nature of ferruginous inclusions in sandstone pebbles (photoes 3a and 3b). The same impact signs are found in ferruginous inclusions in Vendian sandstones [Yurkovets V. P., 2014a].

Fig. 1. Sandstone pebble with a small impact ferruginous inclusions. Kirsino

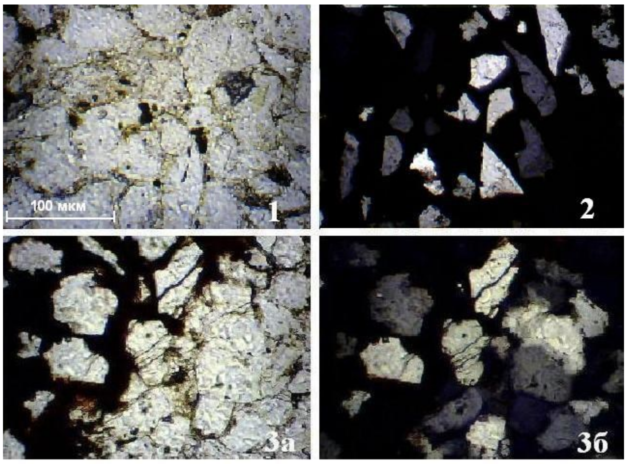

Fig. 2. Parts of thin section No. 259 with quartz grains outside (1), inside (2) ferruginous inclusions and at the boundary of ferruginous inclusion and enclosing mass (3a – plane polarized light, 3b - crossed nicols).

The nature of shock interaction of impact melt fragments and surface of dense crystalline rocks is somewhat different from what is observed in sandstones. There are no ferruginous inclusions formed there, but there are the same signs of shock - crushing, injections of ore components between minerals grains, planar fractures, Isotropization expressed in mosaic extinction of quartz grains in impact zone [Yurkovets V. P., 2015].

According to microprobe analysis in the ferruginous inclusions pyrite predominates. In ferruginous inclusions there is an appreciable amount of secondary sulfates and alkalis - melanterite and jarosite with the ratio of K:Na = 3,24:3,18% [Yurkovets, 2014b].

The foregoing data contain some "reference points" allowing to build the following proposed model of moissanite formation in Ladoga impact process, taking into account composition of the fall area rock.

Melt ejections flying apart from the impact center at a speed of several kilometers per second (required for the formation of diaplectic changes observed in grains of target minerals) occur at the initial stage of transient cavity formation. Predominance of ferruginous component and alkalis is related to selective evaporation of these elements from impact melt [Feldman, 1990].

Since impact melts of ejections are characterized with low degree of mixing and averaging of the original composition [Feldman, 1990], for the purposes of formation of ferruginous inclusions, ShM and moissanite it is necessary to have homogeneous rock complex containing both source of ferruginous inclusions and raw material for moissanite formation. Two such complexes are available in carbonaceous strata of Lyudikoviy and Kaleviy superhorizons of the Upper Kareliy, with total thickness reaching up to 1,700 meters in the Ladoga area. There are horizons with abundant sulfide dissemination and pyrite-pyrrhotite concretions in these strata (Soanlahtinskaya and Zaonezhskaya suites). Also, in these strata there is nearly perfect source for producing moissanite - shungite rocks with silicate mineral base, where shungite content is in the range from 5 to 80%. Schungite contains up to 99% amorphous carbon, which is a strong reducing agent. In this natural "charge" at a temperature of 1800 - 2300 degrees of Celsius (available in impact melt) reaction of silicon dioxide reduction by carbon: SiO2 + 3C = SiC + 2CO, with the formation of a polycrystalline silicon carbide will occur. Subsequent expansion of the gas phase of impact, heated to tens of thousands of degrees, outpacing movement of the melt, will sublimate amorphous SiC, that is already contained therein. Further expansion of the gas phase results in adiabatic fall of its temperature thus creating conditions for the priority (because of its infusibility) crystallization of moissanite. Grains of moissanite along with continuing to expand gas phase, fly apart at a speed of several km / sec forming at collision with rocks shock microstructures (ShM) containing fragments of moissanite - Fig. 3.

The absence of ferruginous components inside Ladoga IVS is caused by the fact that the border of transient crater at all stages of its formation is impact melt from which the selective evaporation of alkalis and iron happens outwards.

The presence of euhedral moissanite in allogenic breccia samples inside the crater [Yurkovets V. P., 2015] indicates its crystallization from the gas phase of impact. That is also indicated by absence of moissanite in melt impactites of Ladoga IVS.

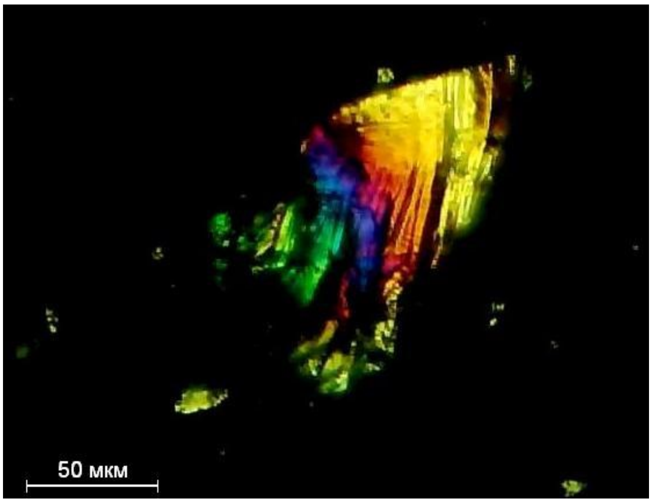

Fig. 3. Thin section No. 13. Catastrophic layers in Kirsino. ShM area with moissanite in sandstone. Crossed nicols

References:

1. Feldman.V.I. 1990. Petrology of impactites. Moscow, Moscow state university publishing house
2. Yurkovets V. P. 2014a. Shock microstructures in rocks of Ladoga IVS. Experimental geochemistry.
3. Yurkovets V. P. 2014b. Signs of impact metamorphism in rocks of Ladoga IVS. Bulletin of the Academy of DNA-Genealogy. Lulu. ISSN 1942-7484
4. Yurkovets V. P. 2015. Extraterrestrial minerals in rocks of the Ladoga region. Proc. VESÈMPG. Editor in Chief A. A. Kadik /Moscow: GEOHI RAS, 2015; 426 p. ISBN 978-5-905049-11-8
5. Ernstson K., Claudin F. 2011. Impact spallation in nature and experiment. http://www.impact-structures.com/2011/12/impact-spallation-in-nature-and-experiment/

Shornikov S. I. Thermodynamics of forsterite evaporation

Vernadsky Institute of Geochemistry and Analytical Chem istry of RAS, Moscow

Abstract. Within the framework of the developed semi-empirical model, the calculations were made of the thermodynamic properties of the $MgO–SiO_2$ melts in the temperature region 2000–2500 K. The calculated values of the partial and total vapor pressures over the $MgO–SiO_2$ melts corresponded to the phase diagram data and showed the incongruent character of forsterite evaporation according to Konovalov's and Vrevsky's rules.

Key words: thermodynamic properties of oxide melts, evaporation, forsterite

Forsterite is the most important chemical compound in the $MgO–SiO_2$ system, which is rarely found in pure form in nature and is part of the olivine group, which represents an isomorphous series of solid solutions in the $Mg_2SiO_4–Fe_2SiO_4$ system. Global distribution of olivine explains the persistent interest to the question of its formation at the earliest stages of the evolution of Solar system matter in the evaporation and condensation processes, and is intensively studied experimentally in the differentiation of matter under high-temperature shock processes and laser heating.

In this regard, the thermodynamic information on the nature of forsterite evaporation has a special interest – namely, the statement on its congruent evaporation in the liquid state [Hashimoto, 1990]. This statement leads to the subsequent important geochemical conclusions. However this statement is in contradiction with the studies of evaporation under the shock processes [Yakovlev et al., 1995] and laser evaporation [Dearnley and Anderson, 1987; Gerasimov et al., 2012].

Consideration of the thermodynamic data, presented in Fig. 1, shows that the temperature dependence of the total vapor pressure over a simple oxide (MgO and SiO_2), which formed forsterite, are close. We can see on Fig. 1, that the total vapor pressure over forsterite close to the same over MgO [Kambayashi and Kato, 1983–1984; Nagahara et al., 1994; Carpenter et al., 2004; Zaitsev et al., 2006]. The results obtained at evaporation of forsterite to Langmuir [Hashimoto, 1990; Nagahara and Ozawa, 1999] are less accurate. Thus, the thermodynamic data on the forsterite evaporation in the liquid state obtained in a single study and

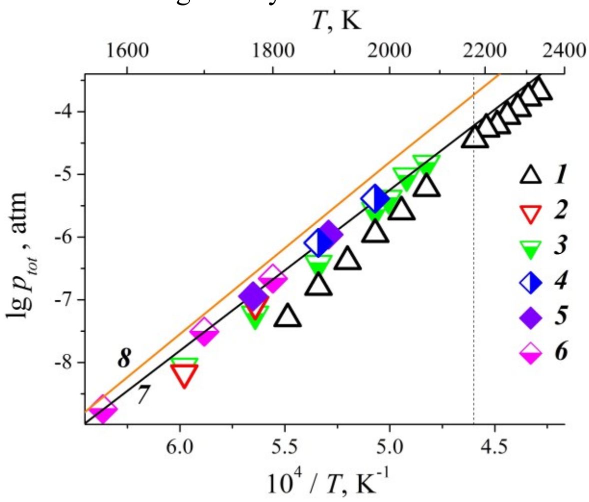

Fig. 1. The total vapor pressure over Mg_2SiO_2 determined: 1 and 2 – to Langmuir [Hashimoto, 1990; Nagahara and Ozawa, 1999], 3–6 – to Knudsen (Nagahara et al., 1994; Kambayashi and Kato, 1983–1984; Stolyarova et al., 2004; Zaitsev et al., 2006], respectively. The total vapor pressure over MgO (7) and SiO_2 (8) calculated in the present study using the data [Glushko et al., 1978–1982; Shornikov et al., 2000]. The dashed vertical line indicates the forsterite melting point.

The present study was supported by RAS Presidium's Program #7 (Experimental and theoretical studies of Solar system objects and star planetary systems. Transients in astrophysics).

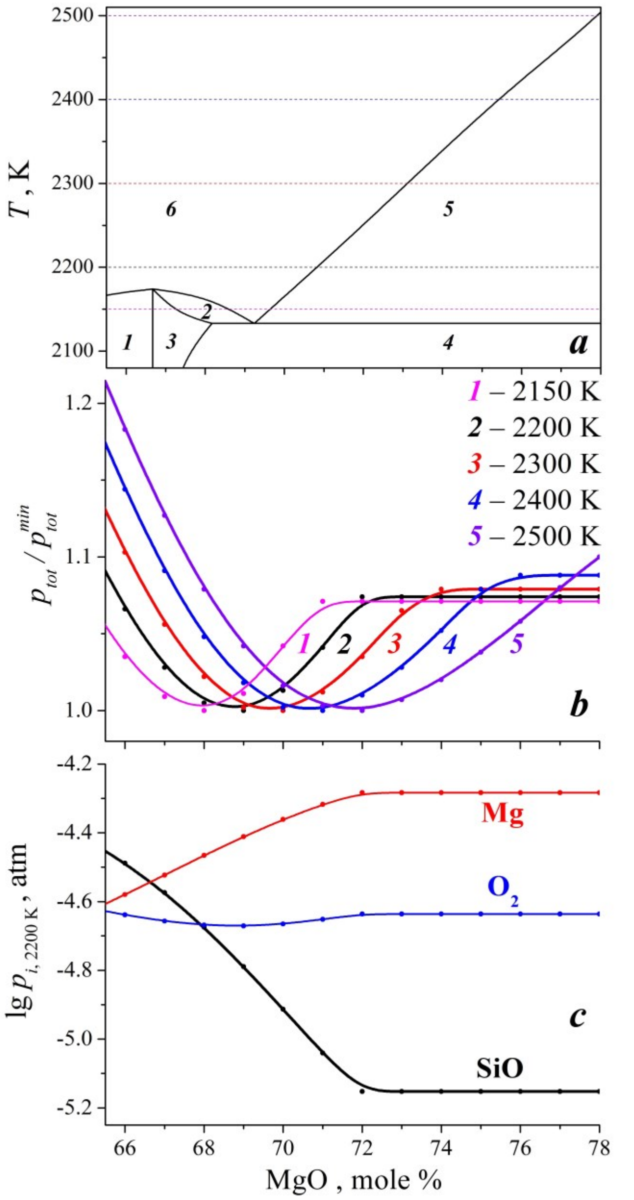

Fig. 2. The phase diagram of the $MgO–SiO_2$ system (*a*), the relative total vapor pressure (*b*) and the partial pressures of vapor species over the $MgO–SiO_2$ melts (*c*). Table of symbols: *1*, *2* – Mg_2SiO_4 + liquid; *3* – Mg_2SiO_4 (solid solution); *4* – Mg_2SiO_4 + MgO; *5* – MgO + liquid; *6* – liquid**.**

In the present study the partial (p_i) and the total vapor pressure (p_{tot}) over the $MgO–SiO_2$ melts in the temperature region of 2000-2500 K were calculated in the framework of the developed semi-empirical model [Shornikov, 2006]. The obtained concentration dependence of p_i and p_{tot} (Fig. 2*b*, *c*) correlated with the phase diagram of the $MgO–SiO_2$ system (Fig. 2*a*), showing the shift of the total vapor pressure minimum to the direction of MgO with the temperature increasing (Fig. 2*b*). It indicate the incongruent nature of forsterite evaporation according to the Konovalov's second rule [Konovalov, 1884] and the Vrevsky's third rule [Vrevsky, 1911].

References:

1. Dearnley, P. A. and K. Anderson (1987). A preliminary evaluation of the potential of laser-beam heating for the production of high melting-point oxide coatings. *J. Mater. Sci*., vol. 22, no. 2, pp. 679–682.
2. Gerasimov, M. V., Yu. P. Dikov, O. I. Yakovlev (2012). Cluster type of silicate vaporization: newly obtained experimental data. *Petrology*, vol. 20, no. 5, pp. 399–407.
3. Glushko, V. P., L. V. Gurvich, G. A. Bergman, I. V. Veitz, V. A. Medvedev, G. A. Khachkuruzov, V. S. Youngman (1978–1982). Thermodynamic properties of individual substances. M.: Nauka.
4. Hashimoto, A. (1990). Evaporation kinetics of forsterite and implications for the early solar nebula. *Nature*, vol. 347, no. 6288, pp. 53–55.
5. Kambayashi, S. and E. Kato (1983). A thermodynamic study of (magnesium oxide + silicon dioxide) by mass spectrometry. *J. Chem. Thermodyn*., vol. 15, no. 6, pp. 701–707.
6. Kambayashi, S. and E. Kato (1984). A thermodynamic study of (magnesium oxide – silicon dioxide) by mass spectrometry at 1973 K. *J. Chem. Thermodyn*., vol. 16, no. 2, pp. 241–248.
7. Konovalov, D. P. (1884). On vapor pressure of solutions / Saint-Petersburg, 75 p. [in Russian].
8. Nagahara, H. and K. Ozawa (1999). Mechanism of forsterite evaporation as inferred from surface microstructures. *Proc. Japan Acad. B*, vol. 75, no. 2, pp. 29–34.
9. Nagahara H., I. Kushiro, B. O. Mysen (1994). Evaporation of olivine: low pressure phase relations of the olivine system and its implication for the origin of chondritic components in the solar nebula. *Geochim. Cosmochim. Acta*, vol. 58, no. 8, pp. 1951–1963.
10. Shornikov, S. I. (2006). Thermodynamic properties of $MgO–SiO_2$ melts. *Experiment in Geosciences*, vol. 13, no. 1, pp. 56–57.
11. Shornikov, S. I., I. Yu. Archakov, M. M. Shultz (2000). Mass spectrometric study of evaporation and thermodynamic properties of silica: III. Equilibrium reactions of molecules occurring in the gas phase over silica. *Russ. J. General Chem*., vol. 70, no. 3, pp. 360–370.
12. Stolyarova, V. L., S. I. Lopatin, V. V. Bondar (2004). Thermodynamic properties of the $MgO–SiO_2$ system by high-temperature mass spectrometry. *Dokl. Phys. Chem*., vol. 399, no. 1, pp. 82–84.
13. Vrevsky, M. S. (1911). On composition and vapor pressure of solutions // Saint-Petersburg, 65 p. [in Russian].
14. Yakovlev, O. I., Yu. P. Dikov, M. V. Gerasimov (1995). Experimental study of shock and pulse evaporation of the ultrabasic substance. *Geochem. Int.*, vol. 33, no. 8, pp. 1235–1248.
15. Zaitsev, A. I., N. A. Arutyunyan, N. G. Shaposhnikov, N. E. Zaitseva, V. T. Burtsev (2006). Experimental study and modeling of the thermodynamic properties of magnesium silicates. *Russ. J. Phys. Chem*., vol. 80, no. 3, pp. 335–344.

Yakovlev O. I. and Shornikov S. I. The evaporation peculiarities of Ca–Al–Inclusions of chondrites

Vernadsky Institute of Geochemistry and Analytical Chemistry of RAS, Moscow

Abstract. Using the D. S. Korginsky's theory of melt acid-base relationship we explained the mutual MgO and SiO_2 evaporation from CAIs melts. Due to activity inversion the MgO evaporation increases and SiO_2 decreases with increasing CaO in residual melts. The real CAIs chemical and isotope compositions are in good agreement with theoretical model.

Key words: evaporation, chondrites, Ca-Al-inclusions, thermodynamic activity

Calcium and aluminium rich inclusions of chondrites (CAIs) are unique geochemistry objects. This substance is called refractory inclusions or Ca–Al–inclusions in the Russian literature. It often refers to short abbreviated form of CAIs (Ca–Al–Inclusions) in English literature. CAIs represent the most primitive matter of the Solar system with the age of 4.567 billion years.

During the high-temperature evaporation of CAIs melts (consisting mainly of SiO_2, MgO, CaO and Al_2O_3 oxides), there are the inversion of the volatility of SiO_2 and MgO. As a matter of fact the silicon oxide being more volatile than magnesium oxide are becoming less volatile under the evaporation conditions of melts inriched of CaO and Al_2O_3 oxides. The volatility inversion is well explained in the framework of the Korginsky's theory of the acid-base interaction of components in silicate melts [Korginsky, 1959]. According to the theory, the increase of the CaO content in the melt of the $CaO–MgO–Al_2O_3–SiO_2$ system leads to increasing of melt basicity, that in turn leads to increasing the MgO thermodinamic activity and volatility, and to decreasing activity and volatility of the SiO_2.

In the first approximation the evaporation process of CAIs melts can be described in terms of the ternary CMAS oxide system. The oxides are divided into the next groups on acid-basic properties: acidic (SiO_2), amphoteric (Al_2O_3) and basic (CaO and MgO). Moreover, the CaO as the main basic oxide of melts, is a major donor to oxygen ions, and its concentration indirectly specifies the basic index of the melts.

It follows:

1) the concentration increasing of calcium oxide in the melt should allow: a) to increase activity and the volatility of MgO, and b) to the drop of the activity and the volatility of SiO_2. The activity calculation carried out according to data [Rein and Chipman, 1965; Shornikov, 2008] illustrates the forecast of the theory and clearly shows the inversion in the activity values of SiO_2 and

MgO, depending on the CaO content in the melt (Fig. 1);

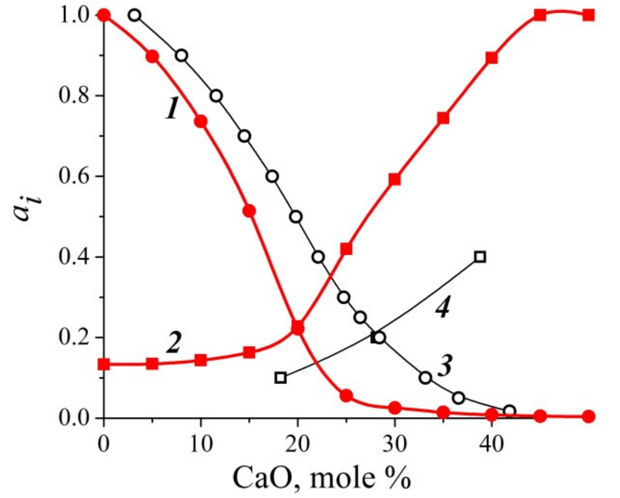

Fig. 1. The activities of SiO_2 (*1*, *3*) and MgO (*2*, *4*) *vs.* the CaO content in the CaO–MgO–SiO_2 system at 1600 °C and MgO : SiO_2 = 2 : 3 mole ratio according to the data: *1* and *2* – [Shornikov, 2008], *3* and *4* – [Rein and Chipman, 1965].

2) during the evaporation the increasing of calcium oxide concentration in the melt should lead to a reduction in the MgO content and relative increase of the SiO_2 content. As a result of this process the ratio of MgO : SiO_2 in the residual melt should decrease, as observed in the real Ca–Al–inclusions (Fig. 2).

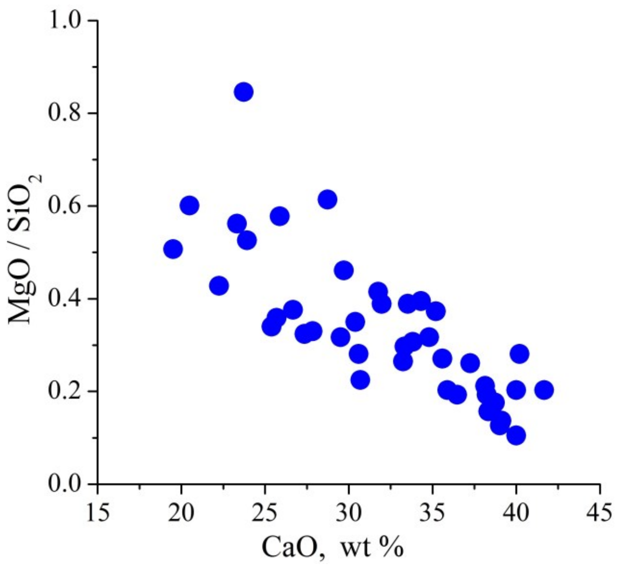

Fig. 2. The dependence of the ratio of MgO and SiO_2 contents in Ca–Al–Inclusions in chondrites *vs.* the CaO content (the correlation coefficient *r* = 0.8).

As shown by the analysis of the isotopic mass fractionation data of magnesium and silicon in the residue after evaporation of the melts [Mendybaev et al., 2013], acid-basic factor has a strong influence on the efficiency of the separation isotopes. Fig. 3 clearly shows that the efficiency of isotope separation of magnesium compared to silicon isotopes in the CMAS melts increases with an increasing content of CaO.

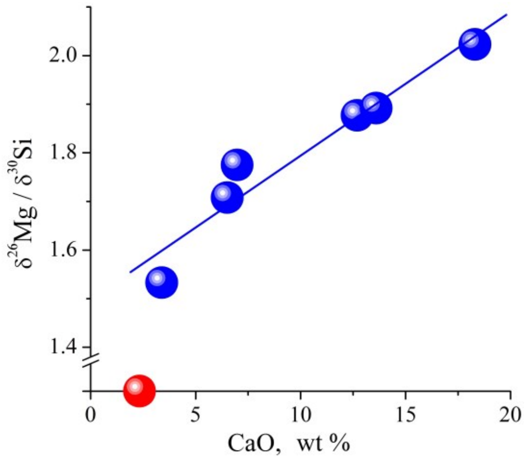

Fig. 3. The fractionation effectivity of the Mg and Si isotopes *vs.* the CaO content. The CaO initial content denoted the red symbol.

The present study was supported by RAS Presidium's Program #7 (Experimental and theoretical studies of Solar system objects and star planetary systems. Transients in astrophysics).

References:

1. Korginsky, D. S. (1959). The acid–base interaction of components in silicate melts and the direction of cotectic lines. *Doklady AN SSSR*, vol. 128, no. 2, pp. 383–386 [in Russian].
2. Mendybaev, R. A., F. M. Richter, R. B. Georg, P. E. Janney, M. J. Spicuzza, A. M. Davis, J. W. Valley (2013). Experimental evaporation of Mg– and Si–rich melts: implications for the origin and evolution of FUN CAIs. *Geochim. Cosmochim. Acta*, vol. 123, pp. 368–384.
3. Rein, R. H. and J. Chipman (1965). Activities in the liquid solution SiO_2–CaO–MgO–Al_2O_3 at 1600 °C. *Trans. Met. Soc. AIME*, vol. 233, no. 2, pp. 415–425.
4. Shornikov, S. I. (2008). Thermodynamic properties of MgO–Al_2O_3–SiO_2 melts. *Experiment in Geosciences*, vol. 15, no. 1, pp. 147–149.

UDC 550.4

Kadik A.A., Koltashev V.V., Kryukova E.B., Tsekhonya T.I., Plotnichenko V.G. Source of oxygen in experimental iron-bearing silicate melts equilibrated with metal phase at high pressures and low oxygen fugacity values.

V.I. Vernadsky Institute RAS, FORC RAS, Moscow (tsekhonya@geokhi.ru)

Abstract. A striking stability of the presence of OH^- groups and molecular water in silicate melts equilibrated with Fe alloy at high pressures and temperatures is

revealed despite the extremely low oxygen fugacity values. In this article the possibility of water formation is considered at FeO reduction from magmatic fluids under the influence of hydrogen.

Keywords: Experiment, Early Earth's mantle, Fe alloy segregation, Oxygen fugacity, Hydrogen, H_2O

The article discusses the reasons for the appearance of oxidized H forms (OH^- and H_2O) in the conditions of extremely low oxygen fugacity (fO_2) values (by 2-4 orders of magnitude below $fO_2(IW)$). The study of solubility of HCNO volatiles in silicate melts equilibrated with Fe alloy at high pressures and fO_2, characteristic of the early Earth's mantle, has revealed a surprising constancy of the presence of hydroxyl OH^- groups and molecular water H_2O in the studied systems (e.g., Mysen et al., 2009, 2011; Mysen, 2012; Kadik et al., 2013; 2014; 2015).

We offer an explanation of the possibility of this property basing, as an example, on the experiments for the system $FeO–Na_2O–SiO_2–Al_2O_3$ in the presence of silicon nitride (Si_3N_4) and graphite as the sources of nitrogen and carbon at $fO_2 < fO_2(IW)$.

The experiments were conducted using an anvil with hole apparatus at 4 GPa and 1550°C. Oxygen fugacity in the experimental sample was controlled by a redox reaction between externally buffered hydrogen and components of Fe-bearing melt, which was reduced with the release of oxygen and metal Fe phase (Kadik et al., 2004; 2013):

$$FeO_{melt}=Fe_{metal}+½\,O_2 \qquad (1)$$

The initial Si_3N_4 is unstable under the experimental conditions and completely consumed via the oxidation reaction

$$Si_3N_{4init}+3O_2=3SiO_{2melt}+2N_{2melt} \qquad (2)$$

with the subsequent participation of nitrogen in the reactions with the components of silicate melt and hydrogen.

To determine the dissolution mechanisms of volatile components in the melts at high temperatures and pressures obtained after quenching the products of the experiment, the glasses were studied by IR and Raman spectroscopy.

The IR spectra of glasses after the experiment at $\Delta fO_2(IW)$ = -3.1 indicate the presence of absorption bands due to stretching vibrations of hydroxyl groups and water. Thus a broad asymmetric absorption band with the peaks at 3632, 3548, 3482 и 3365 cm^{-1} is related to the stretching vibrations of hydroxyl groups OH^- and H_2O molecules (e.g., Stolper, 1982; Dianov, et al., 2000; Mandeville et. al., 2002). The sharp peak at 1620 cm^{-1} corresponds to the bending vibrations of H_2O molecules, and the weak peaks at 4543 и 4972 cm^{-1} are attributed to the stretching vibrations of OH^- and H_2O molecules, respectively. The weak absorption band near 4130 cm^{-1} belongs to the molecular H_2 dissolved in glass.

The Raman spectra also confirm the presence of oxidized forms of hydrogen in glasses (OH^- and H_2O), as well as the molecular H_2 at $\Delta fO_2(IW)$ = -3.1.

In the region 3300-3700 cm^{-1} they contain an asymmetric broad band with a maximum in the frequency range 3566-3571 cm^{-1}, corresponding to stretching vibrations of O-H bonds in OH^- groups and H_2O molecules in the structure of silicate melts. Weak peak at 1615 cm^{-1} is due to bending vibrations of O-H bonds in H_2O molecule dissolved in glass. The band at 4136 cm^{-1} is weakly pronounced and relates to vibrations of H-H bonds in the molecular H_2 in glass (Luth et al., 1987; Plotnichenko et al., 2005).

The absorption coefficients of IR bands (*Abs*) at fO_2 values under study, normalized to the absorption coefficient (Abs^0) for $\Delta \log fO_2(IW)$ = - 1.5, are shown in Fig. 1. With lowering fO_2 in the melt they indicate minor changes in H_2O content and a significant decrease in OH^- content with the corresponding reduction of the total water content (OH^-+H_2O).

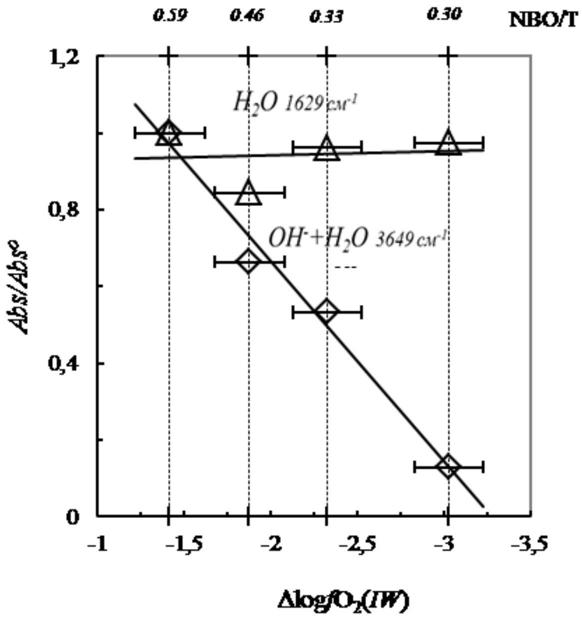

Fig. 1. Influence of fO_2 on the formation of molecules and species OH^-+H_2O (3548 cm^{-1}), H_2O (1620 cm^{-1}) in the melt $FeO–Na_2O–Al_2O_3–SiO_2$ at 4 GPa and 1550°C.

Total water content (OH^- + H_2O) in glasses was determined on the basis of Bouguer–Lambert–Beer's law using Abs^{3548} values from the IR spectra at 3548 cm^{-1} (e.g., Mercier et al., 2010). The molar extinction coefficient ε^{3548} was estimated from its dependence on the structural parameter NBO/T of glass calibrated by Mercier et al. (2010). The obtained (OH^- + H_2O) contents recalculated to H_2O are 2.93, 1.98, 1.65, and 0.41 wt % at $\Delta \log fO_2(IW)$ = -1.5, -1.9, -2.4, and -3.1, respectively.

Knowing the amount of reduced Fe, we calculated the amount of oxygen in the quenching products of experiments (Fig.2.).

The difference between FeO contents in $FeO–Na_2O–SiO_2–Al_2O_3$ melts and in starting silicate mixture (20 wt %) can be used to estimate the amounts of Fe alloy and oxygen formed through the melt reduction (reaction 1) and the amount of oxygen consumed for Si_3N_4 oxidation (reaction 2) (Fig. 2). These estimates indicate that the amount of oxygen produced by FeO reduction is higher than the amount of oxygen necessary for Si oxidation with SiO_2 formation. It can be suggested that the excess oxygen corresponds to its amount consumed by the formation of nitrogen, carbon, and hydrogen species in silicate liquid. The most important component is H_2O. Part of oxygen could be dissolved in Fe alloy (e.g., Ricolleau et al., 2011).

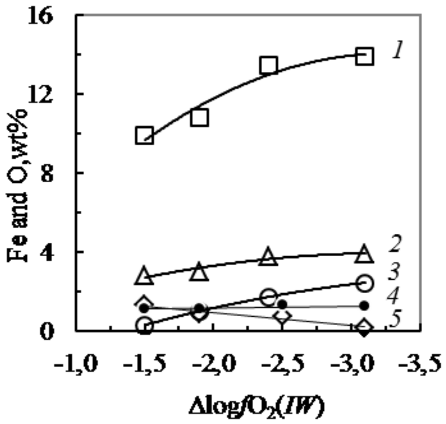

Fig. 2. Balance of oxygen and the amount of reduced Fe in experimental products.

Figure shows the amounts formed during the silicate melt reducing: 1 – amount of metal Fe phase, 2 – amount of O due to the reaction (1); amount of O consumed for: 3 - Si_3N_4 oxidation and SiO_2 formation via the reaction (2), 4 - dissolution in Fe alloy (Ricolleau et al, 2011.); 5 - H_2O formation in the melt.

Thus, the experiments suggest the magmatic environment of the early Earth's mantle favorable for the formation and storage of the released oxygen in it and consider the reaction of FeO reducing from the magmatic liquids under the influence of hydrogen as one of the probable, and perhaps the main mechanisms of its formation.

This work was partially supported by the Program of the Presidium of RAS 22P and RFFI grant 14-05-00136.

References:

1. Dianov et al., 2000. *J. of Non-Crystalline Solids*, **270**, 20-27.
2. Kadik et al., 2004. *J. Petr.* **45** (7), 1297–1310.
3. Kadik et al., 2013. *Phys.Earth Planet.Int.* **214**, 14–24.
4. Kadik et al., 2014. *Geoch.Inter.* **52** (9), 707–725.
5. Kadik et al., 2015. *Geoch.Int.* **53** (11), 867–887.
6. Luth et al., 1987. *Am.Mineral.* **72**, 481–486.
7. Mandeville et. al., 2002. *Am.Mineral* **87**, 813–821.
8. Marty, 2012, *EPSL* **313–314**, 56–66.
9. Mysen B.O., 2012. *Lithos* **148**, 228–246.
10. Mysen et al., 2009. *GCA* **73**, 1696–1710.
11. Mysen et al., 2011. *GCA* **75**, 6183–6199.
12. Mysen, 2012, *Lithos* **148**, 228–246.
13. Plotnichenko et al., 2005. *J. Non-Crystal. Sol.* **351** (49–51), 3677–3684.
14. Ricolleau et al., 2011. *EPSL* **310**, 409–421
15. Stolper, 1982. *CMP* **81**, 1–17.

UDC 523
Kronrod V.A., Kuskov O.L. Фgreement between lunar crustal porosity, thermal conductivity and uranium concentration in the crust and mantle.

V.I. Vernadsky Institute RAS, Moscow
(va_kronrod@mail.ru)

Abstract. The problem of agreement between thermal conductivity coefficient and porosity of the lunar crust and heat source intensities in crust and mantle is discussed. Heat flows and temperature at the depth of lower boundary of the crust satisfy constraints from seismic data. Input parameters of the model are uranium concentrations in crust and mantle, relation between heat conductivity coefficient and porosity, crustal thickness. Constraints on distribution of porosity and heat conductivity coefficients in the crust were obtained. If lunar crust thickness is 34-44 km bulk uranium concentration of the Moon is 15.5-23 ppb and uranium concentration of the crust is 40-200 ppb.

Keywords: Moon, crust, thermal conductivity, porosity, numerical simulation, uranium concentrations

Introduction

The thickness and structure of the lunar crust are key constraints on bulk composition, evolution, and formation of the Moon. The Gravity Recovery and Interior Laboratory (GRAIL) mission is providing unprecedentedly high-resolution gravity data, which provide new information on the thickness, density and porosity in the crust [1]. On the other hand, we obtained surface and mantle heat flow and upper mantle temperature estimations in the Moon with inversion of seismic data into temperature [2, 3]. In this work the results of lunar crust modeling are presented. These results are based on matching of thermal constraints and new information about crustal structure.

Thermal model

Heat transfer in the crust is described by one-dimensional steady-state thermal conductivity equation. At the upper boundary the temperature T_0

$=0^oC$ and heat flow J_0 are defined. Heat flow J_0 is calculated from the average uranium concentration (U_{bulk}) in the Moon with the assumption that ratios Th/U and K/U are standard. Heat source intensity in the crust q_{cr} and thermal conductivity coefficient k as a depth (H) function are model parameters. Total average heat source intensity in the crust or average uranium concentration in the crust is defined in the range U_{cr}=40-240 ppb. Besides boundary conditions, the temperature at the lower boundary of the crust and its derivative should satisfy constraints obtained from the calculations of probable temperature profiles in the upper mantle of the Moon: $dT/dH_{crust-mantle} \cong 1.17$ град/км, $T_{crust-mantle} \approx 300^o - 600^o$ C [2, 3].

Porosity

Effective heat conductivity coefficient considerably depends on material porosity. The lunar crust at the depth of 2 to 10 km (probably to several tens km) was formed as a result of multiple fallings of bodies on lunar surface, its impact destruction and fragmentation. The porous layer of mixed in a random way rock fragments (megaregolith) was formed. Porous crustal medium can be represented as a homogeneous two-phase material (rock) with heat conductivity coefficient k and local average density of the material. Porosity distribution (f) in the generally accepted models of the earth's sedimentary rocks is described by the simple exponential function, which depend on mechanical properties of the rock (P_c). P_c is the characteristic closure pressure of the material. We applied similar approach to the lunar crust to choose coefficients in the exponential model with estimating of porosity distribution from gravitational data. [1], fig 1.

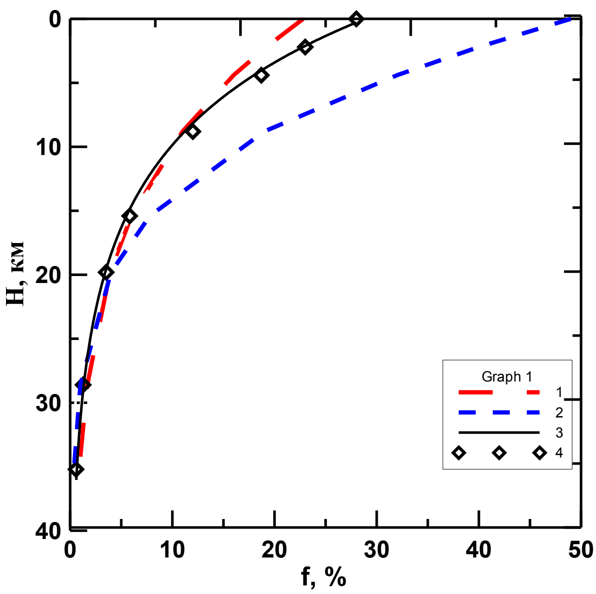

Fig.1. The porosity (f) dependence on depth (H) in the lunar crust. (1) - Pc=300 MPa; f(0)=23%; (2) - Pc=200 MPa; f(0)=49%; (3) - Pc=250 MPa, f(0)=28%; (4) – the model of best approximation from gravitational data [1].

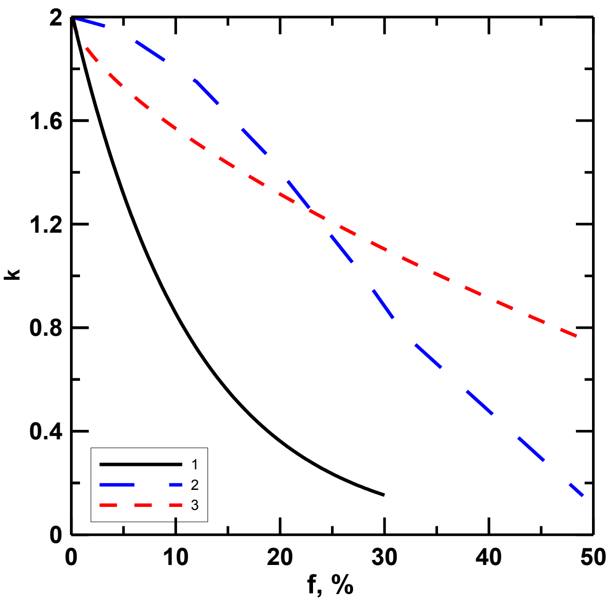

Fig. 2. The heat conductivity coefficient (k) dependence on porosity (f). (1) – approximation of experimental data shown in [4], (2) – model [5]; (3) – geometric model [6].

Heat conductivity

To calculate temperature profiles one must have effective heat conductivity coefficient dependence on depth. Laboratory lunar rocks samples experiments show that porosity is very important cause which controls thermal conductivity of the lunar crust. We considered three methods of k calculation (fig. 2). The most successful results were obtained for the model with approximation of experimental data shown in [4].

Heat generation in the crust

Heat generation in the unit of volume in the crust depends on porosity and concentration of radioactive elements in the matter. In our model exponential mass heat source intensity ($q_m(z)$) distribution with depth was accepted (fig. 3), H_e – the depth where intensity decreases in ***e*** times.

Constraints on the physical properties in the crust

The calculation of the temperature field in the crust revealed that the most strict restriction on the model was the condition $T_{crust-mantle} \geq 300$ C^o, which can be satisfied only in case of very low values of k in the upper layers of the crust. The requirement of low values of k leads to strict restrictions on porosity, fig.2. The porosity distribution should in turn satisfy the data from gravitational estimations, fig. 1. The temperature profile is also affected by the distribution of heat sources in the mantle which depends on the porosity and H_e. To satisfy all these constraints many numerical experiments have been made. It was revealed that the models of the crust with porosity on the surface f≅28% function f(H), which is in agreement with gravitational data (fig. 1), dependence k(f) obtained by the approximation of experimental data (fig. 2), value of $H_e \approx 30$ km, closure pressure $P_c \cong 250$ MPa satisfy all given constraints.

Uranium concentration in the mantle

Model parameters calculated enable us to obtain tolerance range of bulk concentration U_{bulk} and mean concentration in the crust U_{cr}, fig. 4. In case of crust depth 34 km U_{bulk} is in the short range of 20 – 23.5 ppb and U_{cr} =125 – 210 ppb; if H_{cr}=34 km - U_{bulk}=17-22.5 ppb, U_{cr} =60 – 160 ppb correspondingly.

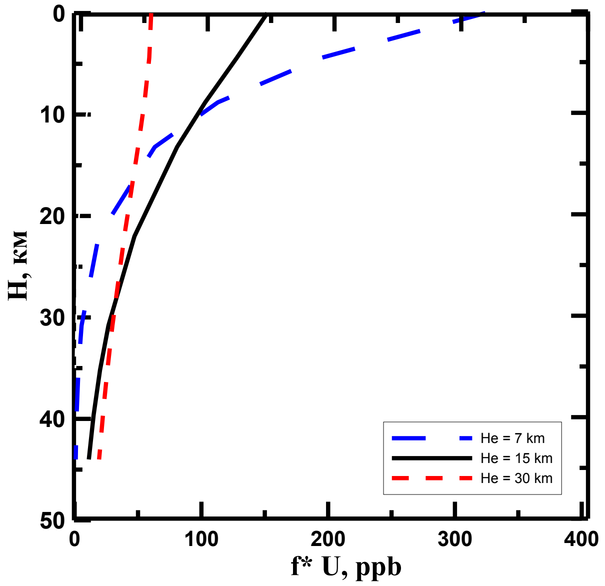

Fig.3. Dependence of uranium concentration U*f with depth H in the lunar crust at different values He. U_{cr}= 60 ppb.

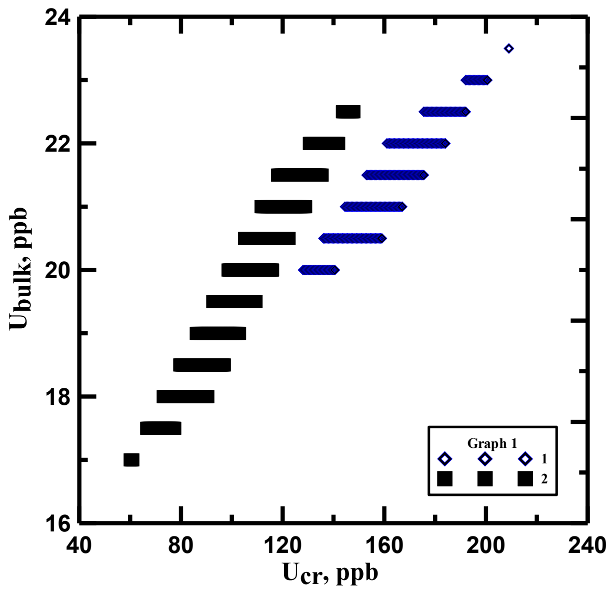

Fig.4. Dependence between bulk uranium concentration U_{bulk} and mean uranium concentration in the crust U_{cr}. $T_{cr\ mantle} \geq 300^oC$. (1) – H_{cr}=34 km; (2) – H_{cr}=44 km

Conclusion

Constraints on the temperature $T_{crust\text{-}mantle} \geq 300^oC$ in case of heat flow $dT/dH|_{crust\text{-}mantle} \cong 1.17$ ^oC/km (H_{cr}=34-44 km) can be satisfied if crust parameters are as follows: porosity on the surface f≅28%, He≈30 км, closure pressure Pc ≅ 250 Mpa. If H_{cr}=34 km bulk uranium concentration is 20 – 23.5 ppb, uranium concentration in the crust - 125 ÷210 ppb; if H_{cr}=44 km, bulk concentration is 17-22.5 ppb and crustal concentration is 60-140 ppb consequently.

Acknowledgments: This research was supported by the RFBR Grant 15-05-0257 2 and Grant 15-05-01161.

References:

1. Besserer J. F. et al. 2014. GRAIL gravity constraints on the vertical and lateral density structure of the lunar crust. Geophys. Res. Lett., 41, doi:10.1002/2014GL060240.
2. Kronrod V. A., Kronrod E. V., Kuskov O. L. 2014. Constraints on the Thermal Regime and Uranium Content in the Moon: Evidence from Seismic Data. Doklady Earth Sciences. V. 455, Part 2, pp. 485–489. http://exp-geochem.ru/JPdf/01_Planetology/01_Rus/29_01_Rus.pdf.
3. Kuskov O.L., V.A. Kronrod, Kronrod E.V. 2014. Thermo-chemical constraints on the interior structure and composition of the lunar mantle. Phys. Earth Planet. Interiors. http://dx.doi.org/10.1016/j.pepi.2014.07.011.
4. Keihm S.J., Langseth M.G. 1977. Lunar thermal regime to 300 km. Proc. Lunar Sci. Conf. 8th p. 499—514.
5. Shoshany Y. D. et al. 2002. Monte Carlo modeling of the thermal conductivity of porous cometary ice. Icarus, 157(1), p. 219–227.
6. Smoluchowski, R. 1981. Amorphous ice and the behavior of cometary nuclei, Astrophys. J., 244, L31–L34.

Lavrentjeva Z.A., Lyul A.Yu. Fractionation of siderophile elements in magnetic grain-sized fractions from Abee EH4, Adhi Kot EH4, Atlanta EL6 and Pillistfer EL6 of enstatite chodrites.

V.I. Vernadsky Institute RAS, Moscow (lavza@mail.ru, ajull@mail.ru)

Abstract. In the present paper the results of elemental abundances in separated grain-sized magnetic fractions from EH and EL groups of enstatite chondrites are reported. From observed features of compositions of magnetic fractions it follows that our siderophile element data accord with this idea that Abee EH4, Adhi Kot EH4, Atlanta EL6, Pillistfer EL6 enstatite chondrites reflect main process – crystallization from impact melts. The origin of such melts is probably to either in situ shock melting or incorporation of impact melt ejecta.

Keywords: magnetic fractions, fractionation of elements, enstatite chondries.

Among known planetary materials, enstatite chondrites are truly a breed apart. They are highly reduced, with < 1 mol percent FeO in their silicates, in contrast to other chondrites as well as Earth, Mars, and Venus, which have FeO contents in the 10 - 40% range [Hertogen J. et al., 1983]. Enstatite chondrites are divided into two main groups, EH and EL, based on high and low abundances of FeNi metal: both groups show a metamorphic sequence from type 3 to 6, similar to that observed in ordinary chondrites [Baedecker P.A. and Wasson J.T., 1975; Sears D.W. 1980].

In the paper the results of elemental abundances in separated grain-sized magnetic fractions from Abee EH4, Adhi Kot EH4, Atlanta EL6, Pillistfer EL6 enstatite chondrites are reported. The main aim of our study is to estimate better the petro genesis of enstatite chondrites of EH и EL groups from studding the trace element distribution in individual grain-sized mineral phases.

Samples and methods

The magnetic fractions were selected by particle – size analysis and handpicking under microscope. The elemental composition of fractions was analyzed at the Central Laboratory of GEOKHI RAS using optimized version of neutron–activation analysis developed for analyzing extraterrestrial material.

Results and discussion

The analysis of the obtained data (Fig. 1) of siderophile elements abundances in the magnetic fractions from Abee EH4 и Adhi Kot EH4 enstatite chondrites showed that behavior of elements were certainly distinctive.

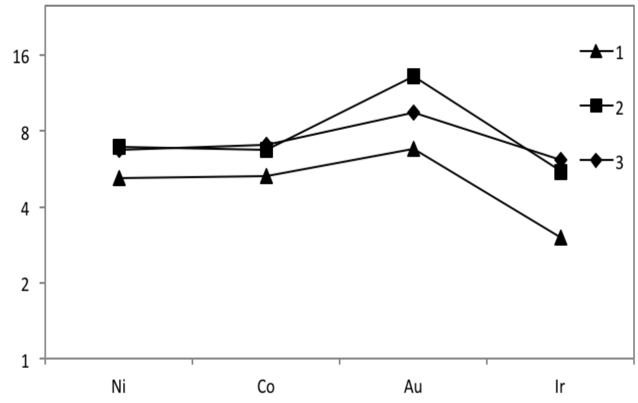

Fig.1. CI chondrite–normalized of siderophile element abundance patterns of magnetic grain-sized fractions 45 <d < 71 µm from enstatite chondrites: 1 - Abee EH4; 2 - Adhi Kot EH4, 3 – average elemental composition metal in E chondrites.

The fractions from Adhi Kot chondrite almost twice as much are enriched in Ni, Co, Au и Ir comparing to their contents in в Abee. Attention is drawn to the much higher content of Au in magnetic grain-sized fraction 45<d<71µm of Abee EH4 chondrite in comparison with their content I Abee EH4 chondrite. The depletion in Au of magnetic fractions from Abee chondrite is probably due to processes of secondary heating and brecciation by impact. These features result from Abee's complex history of shock melting and crystallization. On the base of the features of trace element composition in the magnetic fractions from EH4 group chondrites might be suggested that this elemental fractionation is likely due to by shock with different intensity taking place on parent body of these meteorites.

The EL6 group chondrites differ also in distribution of siderophile elements in magnetic fractions. The lowest concentrations of Co, Au and Ir is observed in fine-grained magnetic fraction from Atlanta EL6 chondrite, and in Pillitfer EL6 chondrite they are consistent with average elemental composition metal in E chondrites (Fig.2).

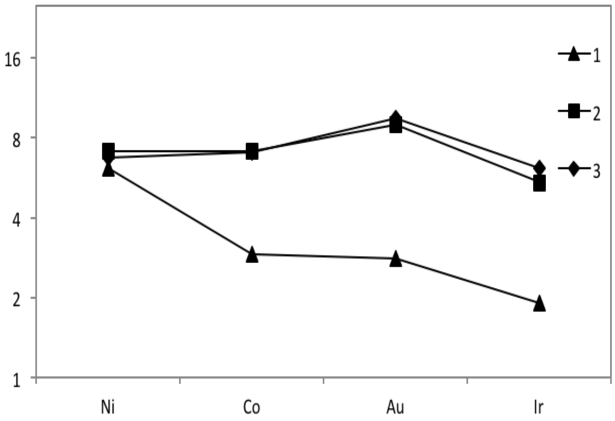

Fig.2. CI chondrite–normalized of siderophile element abundance patterns of magnetic grain-sized fractions 1 <d < 45 µm from enstatite chondrites: 1 – Atlanta EL6, 2 – Pillistfer EL6; 3 – average elemental composition metal in E chondrites.

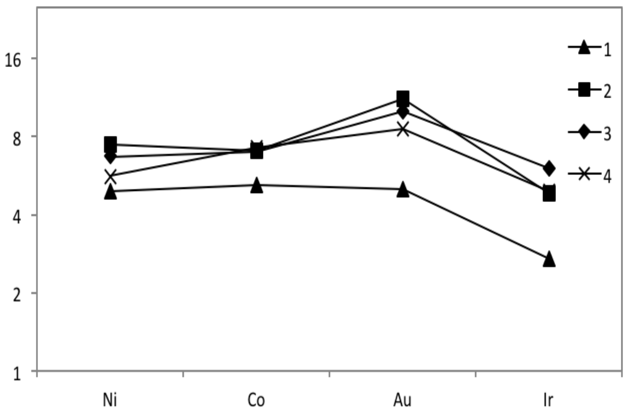

Fig.3. CI chondrite–normalized of siderophile element abundance patterns of magnetic grain-sized fractions 71 <d< 100 µm from enstatite chondrites: 1 - Abee EH4; 2 - Adhi Kot EH4, 3 – Atlanta EL6, 4 – Pillistfer EL6.

The siderophile element abundance in magnetic fractions from Pillistfer EL6 chondrite most approaches to abundances these in bulk metal from E chondrites. Such a distribution of siderophile elements is consistent with the conclusions [Rubin A.E. et al., 1997] that the Pillitfer chondrite experienced the weakly shock. Variations of the relationships $(Ni/Co)_A$ /$(Ni/Co)_{CI}$ = 0.6 – 2.10; $(Ni/Au)_A$ /$(Ni/Au)_{CI}$ = 0.2 – 2.2; $(Ni/Ir)_A$ /$(Ni/Ir)_{CI}$ = 1.0 – 7.5 in the magnetic fractions from Atlanta chondrite indicate that the composition of this fractions different from in Pillistfer chondrite $(Ni/Co)_{П}$ $(Ni/Co)_{CI}$ = 0.8 – 1.0; $(Ni/Au)_{П}$ /$(Ni/Au)_{CI}$ = 0.6 – 0.8; $(Ni/Ir)_{П}$/$(Ni/Ir)_{CI}$ = 1.1 – 1.4.

Iridium – gold relationships in all magnetic fractions from Abee, Adhi Kot, Atlanta and Pillitfer meteorites (Fig. 3.) - $(Ir/Au)_{Abee}$ /$(Ir/Au)_{CI}$ = 0.4 – 0.5; $(Ir/Au)_{Adhi\ Kot}$ /$(Ir/Au)_{CI}$ = 0.4 – 0.5; $Ir/Au)_{Atlanta}$ /$(Ir/Au)_{CI}$ = 0.6 – 0.8; $Ir/Au)_{Pillistfer}$ /$(Ir/Au)_{CI,}$ = 0.5 – 0,7, less than cosmic that indicates the fractionation of these elements in these fractions perhaps by shock-melting of metal. The coexistence of magnetic fractions with the different varieties of elements is consistent with the model of impact destruction of the original body of enstatite meteorites [Okada A. et al., 1988]. From observed differences of compositions of magnetic fractions it follows that our trace element data accord with this idea that this imply co accretion of nebular chondritic components concurrently with hypervelocity impact ejecta, or alternatively, that ejecta was combined with more primitive material during regolith processes [Rubin, 2008].

Conclusions

On the base of the features of siderophile element distribution in grain-sized magnetic fractions from Abee, Adhi Kot, Atlanta and Pillistfer enstatite chondrites one may suggest that many enstatite chondrites have been affected by impact melting and brecciation. Perhaps that such elemental distribution features to have formed by crystallization from impact melts.

References:

1. Baedecker P.A. and Wasson J.T. (1975) Elemental fractionations among enstatite chondrites. 1975. *Geochim. Cosmochim. Acta*. V. 38. P. 735 - 765.
2. Hertogen J., Janssens M-J.,Jakahashi H., Morgan J. W., Anders E. (1983). Enstatite chondrites: trace element clues to their origin. *Geochim. Cosmochim. Acta* V. 47. P. 2241 – 2255.
3. Okada A., Keil K., Taylor G. T., Newsom H. (1988) Igneous history of the aubrite parent asteroid: evidence from Norton County enstatite achondrite. *Meteoritics,* V. *23,* P. *59 – 74.*
4. Rubin A.E., Scott E.D.R., Keil K. (1997). Shock metamorphism of enstatite chondrites. 1997.*Geochim. Cosmochim. Acta*. V. 61. P. 847 - 858.
5. Rubin A. E. (2008). Geochemical, mineralogical and petrological relationships in enstatite chondrites.(2008). *Lunar Planet. Sci. Conf.* XXXIX. # 1114.
6. Sears D.W. (1980). Formation of E chondrites and aubrites - thermodynamic model. *Jcarus* V. 43. P. 184 - 202.

UDC 523.681+552.6

Tselmovich V.A.[1], Kurazhkovskii A.Yu.[1], Kazansky A.Yu.[2], Shchetnikov A.A.[3]

,Research of the holocene events recorded in the peat by the magnetic and microprobe data.

[1] GO "Borok" of IPE RAS, [2] MSU, [3] Institute of the Earth's Crust SB RAS tselm@mail.ru

Abstract. Studying of cores of peat deposits allows obtaining information on dynamics of ecological conditions which took place in the course of peat accumulation. Changes of residual magnetization of 306 samples which are on length of a core of peat deposits in the Holocene selected are studied. Variations of Irs can demonstrate the climatic changes happening in the course of peat accumulation, including connected with the catastrophe phenomena. The horizon of 27 cm formed 795 years ago is enriched with the minerals having either a space, or explosive and volcanic origin. In this case it will be balls from magnetite, kamacite, native: Fe, W, Ti, S, Ag, Bi, corundum with particles of nanodiamonds. In the future we plan to identify also other abnormal layers of it and other cuts of peat. The presented results of magnetic and microscopic research of a core of peat deposits have shown that the method used by us allows obtaining information as about smooth cyclic, and strong short-term impacts on the studied ecosystem.

Keywords: peat deposits, residual magnetization, climatic changes, Holocene, catastrophe phenomena

The research of cores of peat deposits allows to obtain information on dynamics of the ecological conditions taking place in the course of accumulating of peat [1,2]. At the same time samples of peat can save information both about cyclic, and about the short-term catastrophic events exerting impact on an ecosystem condition. The main physical factors influencing a condition of ecosystems are temperature, moisture content and duration of the vegetative period. Under the influence of these factors there is a change of physical properties of the accumulating peat horizons. Measurement of physical properties of the samples of peat which are selected on capacity of the formed thickness in some cases allows to carry out reconstruction of physical conditions in which the researched deposits were created. It should be noted that all reconstruction of the physical parameters influencing an ecosystem are carried out on the basis of indirect measurements. To one of the parameters characterizing peat accumulating conditions can serve magnetization of saturation of samples of peat (Irs) of Measurement of IRS allow to make the conclusion about a ratio of organic and mineral substance in these samples. In fig. 1 the example of changes of IRS of the samples which are selected on length of a core of deposits of peat in the Holocene is given. These deposits were selected from the drained kaltus (the riding swamp) on the delta of the Selenga River (Buryatia) near the Ambassadorial station, (coordinates 52 ° 0'32.29" by NL, 106 °22'21.08" EL). 306 samples are studied. Increase in percentage of mineral substance in samples in comparison with organic substance is the reason of increase of IRS. Such communication of behavior of IRS with amount of mineral substance in samples is easily explainable. Organic substance possesses rather low density and in most cases has no residual magnetization. Enrichment of samples of peat mineral substance leads to growth both Irs, and ρ density. Thus, dynamics of IRS and ρ, reflects changes of mineralogical structure of the researched peat horizons. Presumably availability of mineral substance in peat, and also changes of its percentage can be connected with aeolian transfer. The assumption that the aridization of climate and the intensification of aeolian transfer connected with this process lead to growth of IRS and ρ looks rather logical. Thus, the variations of IRS shown in fig. 1 can demonstrate the climatic changes happening in the course of peat accumulating. Besides, in the lower and upper parts of a core the increased values of IRS and ρ are found. In the first case high values of these parameters demonstrate change of conditions of sedimentation (from lake to marsh). In the upper part of a column high values of IRS are connected with an intensification of the industrial pollution happening now, the age of these horizons doesn't exceed 200 years.

If changes of IRS and happened absolutely synchronously, then in simultaneous measurement of these two parameters there would be no need. However in behavior of these parameters there are distinctions. These distinctions are connected to the fact that the behavior of is defined generally the quantitative changes of mineral substance in samples. Changes of IRS are connected to quantity and a type of the ferromagnetic grains which are present at peat deposits. Microspheres of a technogenic origin (the horizon of 1 cm) are found in high layers. The horizon of 14 cm (~ 560 years ago) differs in existence of a large number of carbon microspheres. And in the horizon of 27 cm surge of values of IRS took place.

Earlier the possibility of microscopic diagnostics of a cosmic dust in peat [3] was shown. The possibility of diagnostics in peat of dust-like particles and other origin isn't excluded. The analysis which is carried out by means of the TESCAN VEGA 2 microprobe showed that depending on a depth of the probed horizons the chemical composition and the form of the mineral particles having residual magnetization is changed. At the same time minerals of a technogenic origin from the upper horizons have explicit differences on composition and the form from minerals of natural genesis. Feature of microspheres of a technogenic origin is the abundance the silicate of particles of various composition of the incomplete form, is frequent with magnetite separation. In the underlying horizons similar particles are absent. Magnetic properties of the lower horizons are connected or to existence of detrital particles of titanium magnetite and haemo ilmenite rows, or the kamacite, Ni is defined by presence of pure Fe, Mt of balls. For example, in the horizon of 27 cm surge of values of IRS took place. The analysis of composition which is carried out by means of SEM "TESCAN VEGA 2" showed that in this horizon the mineralogical composition considerably differs from mineralogical composition of the adjacent horizons. So, magnetic properties of the adjacent horizons are defined generally by availability of magnetites, ilmenites, titanomagnetit and maggemit (minerals which get to a precipitate during corrupting of rocks). The horizon of 27 cm is enriched with the minerals having either a space, or volcanic origin. In this case it is Mt balls, kamacite, native: Fe, W, Ti, S, Ag, Bi, corundum with particles of nanodiamonds. By results of dating 14C AMS this event took place ~ 795 calibrated years ago (in preindustrial time). In aeolian deposits similar minerals either are absent, or meet in the minimum quantities. Thus, features of mineralogical composition of the horizon of 27 cm testify to a short-time (disastrous) event, occurred during its accumulation. Deposits of the horizon of 14 cm have interesting feature. In this horizon it is revealed big the number of carbon microspheres of 5-10 microns in size.

Similar particles in other horizons in such quantity aren't found, their nature is unknown.

The presented results of a petromagnetic research of a core of deposits of peat have shown that the method used by us allows to obtain information as about smooth cyclic, and sharp short-term impacts on the studied ecosystem. Researches by means of the microprobe are labor-consuming and can't be conducted for all studied horizons. In this regard at a research of peat cores we use a combination the petromagnetic and micromineralogical methods.

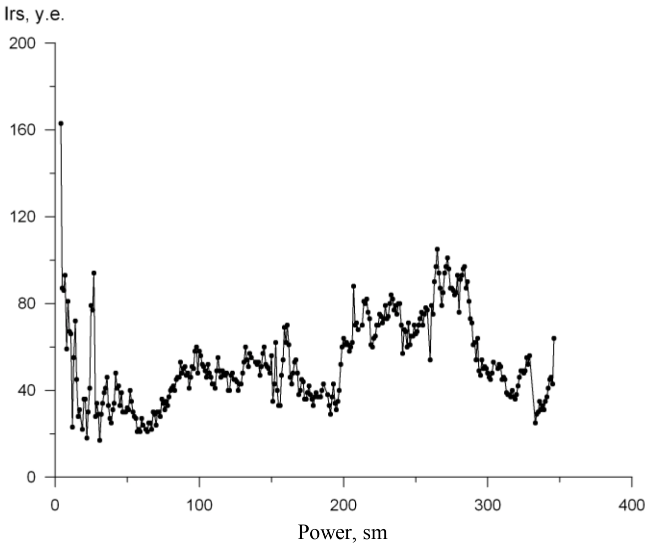

Fig. 1. Variations of IRS in a core of peat deposits.

Work is performed with assistance of the Russian Federal Property Fund, projects 16-05-00703a, 15-05-01644a.

References:

1. Denisenkov V. P. Bolotovedeniye bases. — S-PB.: S.-PGU publishing house, 2000.
2. Lishtvan I. I. Physics and chemistry of peat. – M.: Subsoil, 1989. – Page 304.
3. Tselmovich V. A. Possibilities of microscopic diagnostics of a cosmic dust in peat. "Meteorites, asteroids, comets. Materials of the international conference and school of young scientists CHEBARKUL 2015. ISBN 978-5-9905440-8-6. TETA publishing house, Chelyabinsk. C. 193-196.

Kronrod E.V.[1], Kuskov O.L.[1], Matsumoto K.[2], Yamada R. [2], Computational modeling of the internal structure and composition of the Moon with inversion of gravitational, seismic and geochemical data.

[1] – V.I. Vernadsky Institute RAS, Moscow, [2] – NAOJ, Mizusawa, Japan (e.kronrod@gmail.com)

Abstract. An approach to calculate internal structure and composition (for mantle layers) of the Moon with geochemical, geophysical and selenodetic data inversion was developed. The inversion is based on Bayesian inversion approach and Markov chain Monte Carlo (MCMC) algorithm to infer the parameters of the lunar internal structure. To calculate mantle composition and temperature program code "THERMOSEISM" was used. Models with different input parameters were calculated. Probable seismic velocities distributions, basic oxides concentrations in the mantle and temperature, crustal and LVZ thickness were obtained.

Keywords: Moon, thermodynamics, numerical simulation, internal structure, composition

The goal of our investigation was to obtain geochemically and geophysically consistent information on the internal structure of the Moon.

The problem was to integrate program package THERMOSEISM (calculation of the phase equilibrium and thermodynamic properties) with program developed by RISE project NAOJ Japan which enable us to estimate the internal structure of the Moon from selenodetic and seismic data using method MCMC.

Data and method

The observed parameters in the model were six selenodetic parameters: the mean radius (*R*), mass (*M*), normalized mean solid moment of inertia (*Is/MR*2), degree 2 potential tidal Love number k_2 and monthly and annual quality factors (*Qm* и *Qa*) reported by *Williams and Boggs* [2015], and also 302 seismic data (from 318 data of *Lognonne et al. [2003]*).

A Bayesian inversion approach was used to estimate the internal structure of the Moon. Markov chain Monte Carlo (MCMC) algorithm was used to infer parameters of the lunar structure (layer thickness t, density ρ, shear modulus μ, bulk modulus κ, viscosity η). Temperature and concentrations of the main oxides were estimated in the middle of each layer of the upper, middle and lower mantle with subroutine based on the program package *THERMOSEISM*. From temperature and concentrations the input parameters for the inversion process (ρ, μ and κ) were calculated.

Using parameters ρ, μ, κ, η theoretical values for mass, solid MOI, k_2, *Qm* and *Qa* and seismic travel times can be obtained.

Then, the likelihood function $L(m)$, which is a measure between the model predictions and the observations, were calculated (Matsumoto et al., [2015]).

Thermodynamic approach

To estimate the phase composition and physical properties of the mantle we used program package and database *THERMOSEISM* for the solid-phase seven-component system Na_2O-TiO_2-CaO-FeO-MgO-Al_2O_3-SiO_2 (NaTiCFMAS) with non-ideal solid solutions [Kuskov, 1995, 1997]. The database contains self-consistent thermodynamic parameters of enthalpy, entropy, thermal capacity, Grunaisen parameter, thermal dilatation, shear and bulk modulus for minerals and solid solution interaction parameters (Kuskov, Kronrod, [2001]).

Method of Gibbs free energy minimization and mantle material state equation with phase changes, anharmonicity and anelasticity effects was applied.

State equilibrium calculation for minerals was performed under the quasi-harmonic *Debye–Grüneisen* approximation based on the model of elastic continuum with Born-Mayer potential for the potential part of state equilibrium and Debye approximation for its thermal part.

The model of the Moon

Eight layers models of the Moon are considered: megaregolith layer with the thickness of 1 km, crust, upper mantle, middle mantle, lower mantle, low-viscosity layer (LVZ) with the thickness of 0-500 km, fluid outer core (10–500 km) and solid inner core. The boundaries between upper and middle mantle and middle and lower mantle were at the depths of 500 km and 900 km consequently.

Model input parameters are layer thickness t, density ρ, shear modulus μ, bulk modulus κ, and viscosity η for each layer. For the mantle layers input parameters are main oxides Al, Fe and Mg concentration and temperature T, from which ρ, μ and κ are calculated.

Three variants of the main oxides in the mantle have been considered with wide range of Fe and Mg concentration, same for all three variants: Mg range was 27-45 wt.% for all mantle layers, Fe_1 = 9-13 wt.% in the upper mantle, Fe_2 = 9-14 wt.% in the middle mantle and Fe_3=9-15 wt.% in the lower mantle. Al content in the upper mantle was also the same for all variants: Al_1 = 1-3 wt.%. The difference was in Al concentration in the middle (Al_2) and in the lower (Al_3) mantle (Al_2):

a) Al_2 = 3 - 4,5; Al_3 = 4,5 – 6
b) Al_2 = 4 - 5,5; Al_3 = 5,5 – 7
c) Al_2 = 5 - 7; Al_3 = 6,5 – 8,5

(a) Al content is close to that for the Earth, in (b) and (c) Al content is higher than Earth's value.

Results

The range of models of the Moon with different input parameters was obtained. Probable seismic velocities, concentrations of main oxides in the mantle and temperature range were calculated (Fig.1).

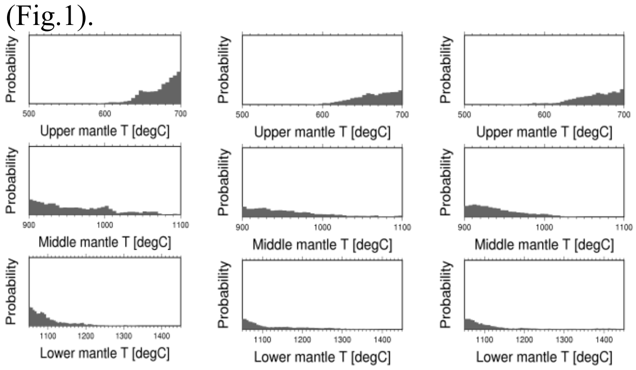

Fig. 1 Probable temperature distribution of the main oxides in the lunar mantle for cases a, b, c

Conclusions

The preliminary estimations of the main oxides concentrations and temperature in the three mantle layers was obtained: in the upper mantle MgO 27-28 wt%, FeO 12,5-13 wt%, Al_2O_3 1-2,5 wt%, in the middle mantle MgO 28-38 wt%, FeO 10-14 wt%, Al_2O_3 4-7 wt%, in the lower mantle MgO 34-44 wt%, FeO 9-15 wt%, Al_2O_3 4,5-8,5 wt%; the temperature in the upper mantle 600-700 ^oC, in the middle mantle 900-1000 ^oC, in the lower mantle 1000-1100 ^oC. Density in the upeer mantle 3,3-3,35 g/cm^3, in the middle mantle 3,35-3,5 g/cm^3, in the lower mantle 3,4-3,5 g/cm^3.

This research was supported by the RFBR grant 15-05-0257 2 and 15-05-01161 and grant of ＜制度名＞ supported by the Research Coordination Committee, National Astronomical Observatory of Japan (NAOJ)

References:

1. Kuskov O.L. 1995. Constitution of the Moon: 3.
2. Composition of middle mantle from seismic data - Phys. Earth Planet. Inter.
3. Kuskov O.L. 1997. Constitution of the Moon: 4.
4. Composition of the mantle from seismic data - Phys. Earth Planet.Inter.
5. Kuskov O.L., Kronrod V.A. 2001. Core sizes and
6. internal structure of the Earth's and Jupiter's satellites - Icarus.
7. Lognonné P. et al. 2003. A new seismic model
8. of the Moon: implications for structure, thermal evolution and formation of the Moon - Earth Planet. Sci. Lett.
9. Matsumoto et al. 2015. Internal structure of the
10. Moon inferred from Apollo seismic
11. data and selenodetic data fromGRAIL and LLR - Geophysical Research Letters
12. Williams, J. G., and D. H. Boggs. 2015. Tides on the Moon: Theory and determination of dissipation - J. Geophys. Res. Planets

Dunaeva A.N., Kronrod V.A., Kuskov O.L. Thermal stability conditions for the internal ocean in the models of partially differentiated satellites Callisto and Titan.

V.I. Vernadsky Institute RAS, Moscow
(dunaeva.an@gmail.com)

Abstract. In this paper we investigated the thermal conditions of the rock-ice mantle and internal ocean existence in the models of partially differentiated satellites Callisto and Titan. It has been shown that the models of the satellites with rock-ice mantle and internal ocean are realized in the range of heat flux values (F) of 3.3<F<14.8 mW/m^2 for Titan and of 2.6<F<4.2 mW/m^2 for Callisto. An additional restriction to Titan's heat flux values could be the density inversion in the outer I*h*-ice crust observed during the model assessments. Such inversion leads to the reduction of permissible range of Titan's heat fluxes to values of 3.3<F<7.1 mW/m^2.

Keywords: Titan, Callisto, heat flux, internal structure

Icy satellites Titan and Callisto belong to different planetary systems; however, they have a number of common features. The satellites occupy a comparatively remote (low temperature) position relative to their central planets, have similar physical characteristics (size, mass, density), contain approximately equal amounts of water and rock material of the same composition, they are characterized by close values of the moments of inertia and probably have identical internal structure.

Among the possible versions of the internal structure of Callisto and Titan a model of partially differentiated satellites was considered [Kuskov, Kronrod, 2005; Dunaeva et al., 2016]. According to this model the satellites were assumed to consist of three major structural domains: the outermost water-ice shell, which contains a liquid aqueous layer (internal ocean), intermediate undifferentiated rock-ice mantle and the central rock-iron core.

Significant restrictions on the application of such model are the values of the satellites' heat fluxes (F), which determine the stability of the rock-ice mantle (solid state of H_2O-phases), as well as the existence and depths of the inner ocean and the thickness of the outer icy crust. Since Callisto's and Titan's heat fluxes values available from literature data are estimated roughly, in this study we investigated all possible range of satellites' heat fluxes values (F), which pose the suitable thermal condition inside satellites' interiors to keep stability of the ice-rock mantle and existence of the internal ocean. Thus, the task was to determine the range of acceptable values of heat fluxes, which provide simultaneous observance of two conditions - existence within the satellites' water-ice shell of a non-freezing watery ocean and stability of crystalline water ices as a part of the satellites' rock-ice mantle.

The development of the models of Callisto's and Titan's internal structure was conducted for the moments of inertia of the satellites $I/MR^2 = 0.3549$ [Anderson et al., 2001] and $I/MR^2 = 0.3414$ [Iess et al., 2010], respectively. The density of water ices and liquid water in the water-ice shell and rock-ice mantle was determined by the individual H_2O-phases equations of state. Changing of the rock component density in the satellites' rock-ice mantle and inner rocky core was estimated by the silica substance equation of state [Castillo-Rogez, Lunine, 2010]. The values of Callisto's and Titan's heat fluxes were calculated using the steady state heat conduction equation for the satellites' outer conductive Ih-ice crust [Kuskov, Kronrod, 2005].

Thermal constraints on the models of partially differentiated Titan

The results of conducted calculations show that within the confines of the chosen model and its limitations Titan's heat flux varies in the range of $3.3<F<14.8$ mW/m^2. The higher heat fluxes lead to melting of the ice mantle, the lower ones lead to freezing of the internal ocean. This means that in the models of partially differentiated Titan the maximum permissible size of the satellite's outer Ih-crust could change in the range of $160>H_{Ih}>80$ km and the depth of the inner ocean does not exceed 420 km (Fig. 1a).

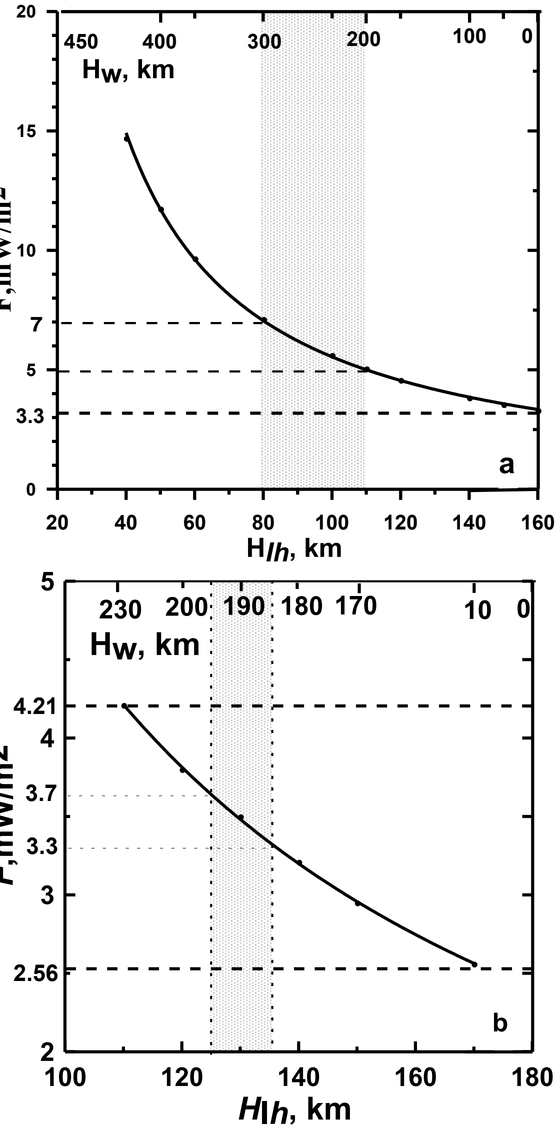

Fig. 1. Thickness of the Ih-icy crust (H_{Ih}) and depth of the internal ocean (H_w) of Titan (a) and Callisto (b) in the range of acceptable values of the satellites' heat fluxes (F).

At the same time the performed calculations showed that at high F values a slight density inversion within Titan's outer Ih-ice crust occurs, which leads to the negative gradient of the ice density with depth ($d\rho/dh<0$). In such a case the thinner the satellite's Ih-crust is and the deeper its internal ocean is, the higher the probability of such inversion occurrence is. The negative density gradients existence can lead to violations of the icy crust stability with imposing of some external factors (for example, with the exposure of the satellite to tidal effects and related ice perturbation within icy shell). The stability criteria of such system require further investigation, but at this stage of the work it is assumed that the density inversion indicates the non-physical values of Titan's heat fluxes. It allows to formulate an additional restriction on range of permissible F-values in the satellite, namely, the absence of ice density inversion with depth. Incorporation of this limitation leads to Titan's heat fluxes not higher than 7.13 mW/m^2, which is in a good agreement with estimates of F = 5-7 mW/m^2, obtained by [Lorenz, 2002; Mitri, 2008]. Thus, we can conclude that the possible thickness of Titan's icy crust in present is from 80 to 110 km, and the depth of the internal ocean is about 200-320 km (gray area in Fig. 1a).

Thermal constraints on the Callisto models

For partially differentiated Callisto the possibility of the internal ocean and rock-ice mantle existence is realized in a fairly narrow range of heat flux values - from 2.6 mW/m^2 to 4.2 mW/m^2. At such heat fluxes the satellite's outer Ih-ice crust is relatively thick (at least 110 km) and the depth of the internal ocean is less than 230 km (Fig. 1b). It has been shown that at the obtained range of valid F-values and at corresponding parameters of the water-ice shell the density inversion in the satellite's outer ice crust does not occur. The current estimates of Callisto's heat fluxes give approximate values of F equal to 3.3-3.7 mW/m^2 [Kronrod, Kuskov, 2003], which corresponds to the thickness of the Ih-icy crust of 125-135 km, with a depth of the internal ocean of 185-195 km (gray area in Fig. 1b).

Main conclusions:

- In the framework of the partially differentiated model of Callisto and Titan the satellites' heat fluxes vary in the range of $2.6<F<4.2$ mW/m^2 and $3.3<F<14.8$ mW/m^2, respectively.
- Taking into account the additional condition that the ice density inversion in Titan’s icy crust is absent, the maximum value of Titan's heat flux can be reduced to 7.13 mW/m^2.
- Depending on the heat flux value the permissible thickness of Titan's outer Ih-ice crust is about of 160>HIh>40 km, the thickness of the Ih-crust of Callisto is $170>H_{Ih}>110$ km.
- At the current estimates of Titan's and Callisto's heat fluxes of 5-7 mW/m^2 and 3.3-3.7 mW/m^2, the satellites' outer Ih-ice crust is 80-110 km and 125-136 km, and the thickness of the internal oceans reaches 200-320 km and 185-195 km, respectively.

This research was supported by the RFBR grant 15-05-02572.

References:

1. Dunaeva A.N., Kronrod V.A., Kuskov O.L. // Geochemistry International, 2016, 54(1), 27-47.
2. Anderson J.D., et al. // Icarus, 2001,153, 157–161.
3. Castillo-Rogez J.C., Lunine J.I. // Geophys. Res. Lett., 2010, 37, L20205.
4. Iess L. et al. // Science, 2010, 327, 1367-1369.
5. Kuskov O.L., Kronrod V.A. // Solar System Research, 2005, 39(4), 283-301.
6. Lorenz R.D. // Icarus, 2002, 156(1), 176-183.
7. Mitri G., Showman A. // Icarus, 2008, 193, 387–396.

Shpekin M.I. [1], Barenbaum A.A. [2] ,On two physical mechanisms interaction of galactic comets with terrestrial planets

[1] Kazan Federal University, Kazan
[2] Oil and Gas Research Institute RAS, Moscow

Abstract. Using theoretical models MA Lavrent'ev we found that the interaction of galactic comets with planets can occur by two different physical mechanisms. According to the first mechanism, the main part of kinetic energy and momentum of the comet is spent on the creation of the crater by diameter in many kilometers. In the second mechanism the energy and momentum of comets are transferred to the narrowly focused shock wave that penetrates deep into the lithosphere, expending energy on evaporation, melting and heating the rocks. On the example of the Earth, Mars, Mercury and the Moon it is shown that galactic comets interact with planets with the participation of both mechanisms. Ceteris paribus the thermal effect increases with the density of the planet's atmosphere.

Keywords: galactic comets, terrestrial planets, mechanisms interaction comets with planets.

Citation: Shpekin M.I., Barenbaum A.A. (2016). On two physical mechanisms interaction of galactic comets with terrestrial planets, *Experiment in Geosciences*. V.22 . No 1

It is known that in resulted of fall galactic comets on the surface of planets the pressure can appear so large that we can neglect of strength and plastic properties of medium and also friction forces in comparison with the inertial forces. In accordance with the idealized hydrodynamic models [Lavrent’ev, 1957, 1959] collision process can take place by physically different mechanisms of "elastic" and "inelastic" impact.

In the case of "elastic" impact, most part of the kinetic energy and the momentum of the comets are spent on the crater formation and the emission of rock fragments from the crater [Melosh, 1989]. If impact is "inelastic" collision energy and the momentum of the comets are passed narrowly focused shock wave, which can penetrate deep into the lithosphere of the planet, expending energy at evaporation, melting and heating the rocks [Barenbaum, 2010, 2012, 2013, 2013a, 2015]. This thermal energy accumulating in the asthenosphere and then is expended into the tectonic, magmatic and geodynamic processes [Barenbaum et al. 2004].

On the example of Earth, Mars, Mercury and the Moon shown [Barenbaum, 2014; Barenbaum, Shpekin, 2016] that high-speed galactic comets interact with the planets with participation of both mechanisms. Moreover at increasing the density of the planetary atmospheric, the heating effect increases. In general case the result of the interaction of galactic comets with planets depends on a combination of four main factors: 1) the presence and density of the gaseous envelope of the planet, 2) layer thickness of the lithosphere rocks, 3) material composition and rock temperature, and 4) the frequency of falls of galactic comets [Barenbaum, 2015b].

Main conclusions:

- Earth and Venus, characterized by a dense gaseous envelope, interact with galactic comets by the physical model of "inelastic" impact. While on the planets with no atmosphere (Mercury, Moon), or with a very tenuous atmosphere (Mars) an important role plays the mechanism of "elastic" impact.
- Falls of galactic comets lead to heating asthenosphere layer of rocks that causes the rise of the surface in the districts subjected cometary bombardment. These elevated areas on the terrestrial planets are considered as "continents".
- In the periods of time between the cometary bombardments (~ 20-30 million years), the heated rocks in asthenosphere are cooled. In a result the height of the continents is reduced, and the irregularities of continental surface are leveled by relaxation processes. Such low-lying places in the relief of the surface Mars, Mercury and Moon are called "marine".
- Due to the orbital motion of the Sun in Galaxy, the galactic comets bombard on alternately as the northern so and southern hemisphere of the planets, that causes in both hemispheres convert of the continental landforms in marine and vice versa [Barenbaum, 2002, 2004, 2012a].
- Last time (epoch from 5 to 1 million years ago) galactic comets bombarded the southern hemisphere of all the planets. We connect with this fact, that the height of the southern hemisphere observed on Mars, Mercury and the Moon in average higher than the northern hemisphere where seas occupy most of the surface area [Yakovkin, 1934; Shakirov, 1963; Rodionova, Dehtyareva, 1986]. It is interesting to note that selenographic map of the places fall for the comet from the Kuiper belt or the Oort cloud built by (Shevchenko, 1996) shows the same attraction the places fall to the southern hemisphere.
- In the crater Tsiolkovsky on the far side of Moon there is clear evidence [Shpekin, 2009; Barenbaum, Shpekin, 2013, 2016] of presence in the past of liquid water and vapor. This fact gives grounds to believe that during the last cometary bombardment on the Moon could be an atmosphere, which was able to hold the water from evaporating galactic comets.

In this article the authors have raised the question of two different physical mechanisms of interaction of the galactic comets with planets. This question is posed by us for the first time and is still far from a final decision. Therefore the conclusions set out by us relating both mechanisms require additional confirmation and further theoretical studying.

References:

1. Barenbaum A.A. (2002) Estimation of tectonic relaxation time of Mars surface using large asteroid craters distribution, *Microsymposium 36 Vernadsky -Brown* . MS004.
2. Barenbaum A.A. (2004). On a feature of the asthenosphere Mars // *Vestnik ONZ RAN* №1(22)'2004 URL: http://www.scgis.ru/russian/cp1251/h_dgggms/1-2004/informbul-1/planet-14.pdf.
3. Barenbaum A.A., V.E. Chain, N.A. Yasamanov (2004). Large-scale tectonic cycles: an analysis from standpoint of galactic concept, *Vestnik MGU*, Ser.4. Geology, №3, pp. 3-16.
4. Barenbaum A.A. (2010). *Galaxycentric paradigm in geology and astronomy* (Moscow: PH LIBROKOM), 544 p. (in Russian).
5. Barenbaum A.A. (2012). On the origin recent uplifts the crust. New formulation of problems global geodynamics, *Uralian Geological Journal*, № 6 (90), pp. 3-26. (in Russian).
6. Barenbaum A.A. (2012a). On the asymmetry of the surface terrestrial planets caused by the falls of galactic comets, *Experiment in Geosciences,* v.18 (1), pp. 8-11.
7. Barenbaum A.A. (2013). On the mechanism of heating lithosphere rocks by galactic comets, *Experiment in Geosciences*, v.19 (1), pp.13-16.
8. Barenbaum A.A. (2013a). A possible mechanism of heating lithosphere rocks galactic comets, *Uralian Geological Journal*, № 1(91), pp. 21-39, (in Russian).
9. Barenbaum A.A, M.I. Shpekin (2013). Impact craters Tsiolkovsky and Aitken as objects of search for residual water on the Moon, *Fourth Moscow Solar System Symp.* (14-18 Oct. 2013, Moscow: Space Research Institute RAS) 4MS3-PS-17 abst.
10. Barenbaum A.A. (2014) Tectonomagmatic consequences of falls galactic comets on the terrestrial planets, *Experimental Geochemistry*, v.2, №1, pp. 20-26.
11. Barenbaum A.A. (2015) Mechanism of formation asthenosphere of terrestrial planets, *Trudy VESEMPG-2015*, v.2, pp. 219-228.
12. Barenbaum A.A. (2015a). On the mechanism of energy dissipation of galactic comets bombarding terrestrial planets, *Journal Physics: Conf. Ser.* 653 012073, doi:10.1088/1742-6596/653/1/012073
13. Barenbaum A.A. (2015b). Formation of analogous geological structures on terrestrial planets by Galaxy's comets, *The Sixth Moscow Solar System Symp.,* (5-9 October 2015, Moscow: Space Research Institute RAS), 6MS3-PS-38, 6MS3-PS-39 abst.
14. Barenbaum A.A, M.I. Shpekin (2016). On two mechanisms of interaction of high speed cosmic bodies with surface planets, *XXI International Conference on Equations of* State for Mater (March 1-6., Elbrus, Russia), Book of Abstracts, (Moscow & Chernogolovka & Nalchik), pp.223.
15. Lavrent'ev M.A. (1957) Cumulative charge and the principles of its operation, *Uspekhi matematicheskikh nauk*, v.12, 4 (76), pp. 41-56.
16. Lavrent'ev MA (1959) Problems at penetration speeds, *Iskusstvennyye sputniki Zemli* (Moscow, Publishing House of the USSR Academy of Sciences), v.3, pp. 61-65.
17. Melosh H. J. (1989). Impact Cratering: Geological Process. Oxford monographs on Geology and Geophysics - N.Y.: Oxford University Press Inc.
18. Rodionova J.F., K.I. Dehtyareva (1986). Hypsometric features of Moon and terrestrial planets, *Problems of a comprehensive study of the Moon* (Moscow: Moscow State University), pp. 56-71, (in Russian).
19. Shakirov K.S. (1962). Experience the definition of permanent rotation of the Moon on the meridian observations of the crater Mësting A, *Astron. Circular*, №231.
20. Shevchenko V.V. (1996). Swirl patterns on the Moon as traces of comet shower, *Astronomichesky Vestnik*, V. 30, N 1, pp. 59-73. (in Russian).
21. Shpekin M.I. (2009). The Last "Apollo" Orbit Pass over the Tsiolkovsky Crater, *Intern. Conf. "Astronomy and World Heritage: Across Time and Continents*" (August 19-26, 2009, Kazan, Russia), pp. 219-221.
22. Yakovkin A.A. (1934). The radius and shape of the Moon, *Bull. Astronomical Observatory. V.P. Engelhardt at Kazan University,* (Kazan).